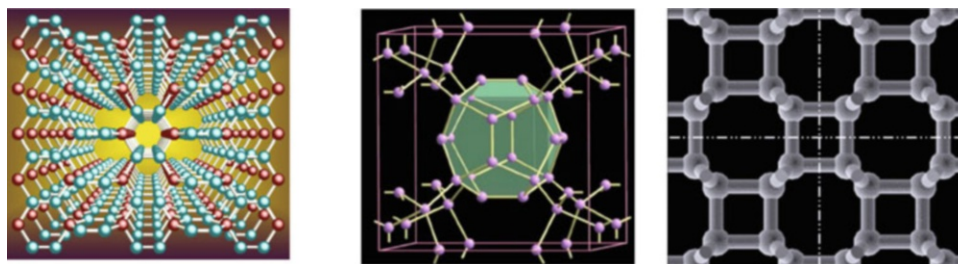# Chapter 6
Predicted Carbon Forms

As it has been shown above, a grand variety of carbon allotropes and forms is currently known. They can be very common (graphite, coal) or rare (nanoplates or nanocups) and can be well-developed industrially (carbon black) or intensively studied on nano-level (carbon nanotubes or graphene), doped with metals and functionalized with organic and organometallic moieties. At the same time, applying modern computational methods, a host of new carbon nanoforms (e.g., novamene [1] or protomene [2]) are possible, which have not yet been observed experimentally. An efficient and reliable methodology for crystal structure prediction was developed [3], merging ab initio total energy calculations and a specifically devised evolutionary algorithm. This method allows one to predict the most stable crystal structure and a number of low-energy metastable structures for a given compound at any *P-T* conditions without requiring any experimental input. While in many cases it is possible to solve crystal structure from experimental data, theoretical structure prediction is crucially important for several reasons.

1.	When experimental data are of poor quality for structure solution (defective or small samples, especially at high pressures and temperatures), theory provides the last resort.
2.	Theory is the only way of investigating matter at conditions that cannot be studied with today's experimental techniques, e.g., at ultrahigh pressures.
3.	The ability to predict crystal structures will open up new ways of materials design.

Several carbon allotropes have been predicted, in particular M-carbon [4], F-carbon [5], orthorhombic W-carbon [6], Z-carbon [7], H-carbon and S-carbon [8], *Imma*-carbon [9], M585-carbon [10], T12-carbon [11], C2/m-16 carbon [12], P222$_1$-carbon [13], Cco-carbon [14], and so on. But only Z-carbon-1, Z-carbon-2, Z-carbon-3, Z-carbon-7, and Z-carbon-10 are potential superhard materials (Fig. 6.1), unlike Z-carbon-5 and Z-carbon-6 which have a hardness of 34.1 GPa and 34.2 GPa, respectively. In this section, we present several representative predicted carbon allotropes.
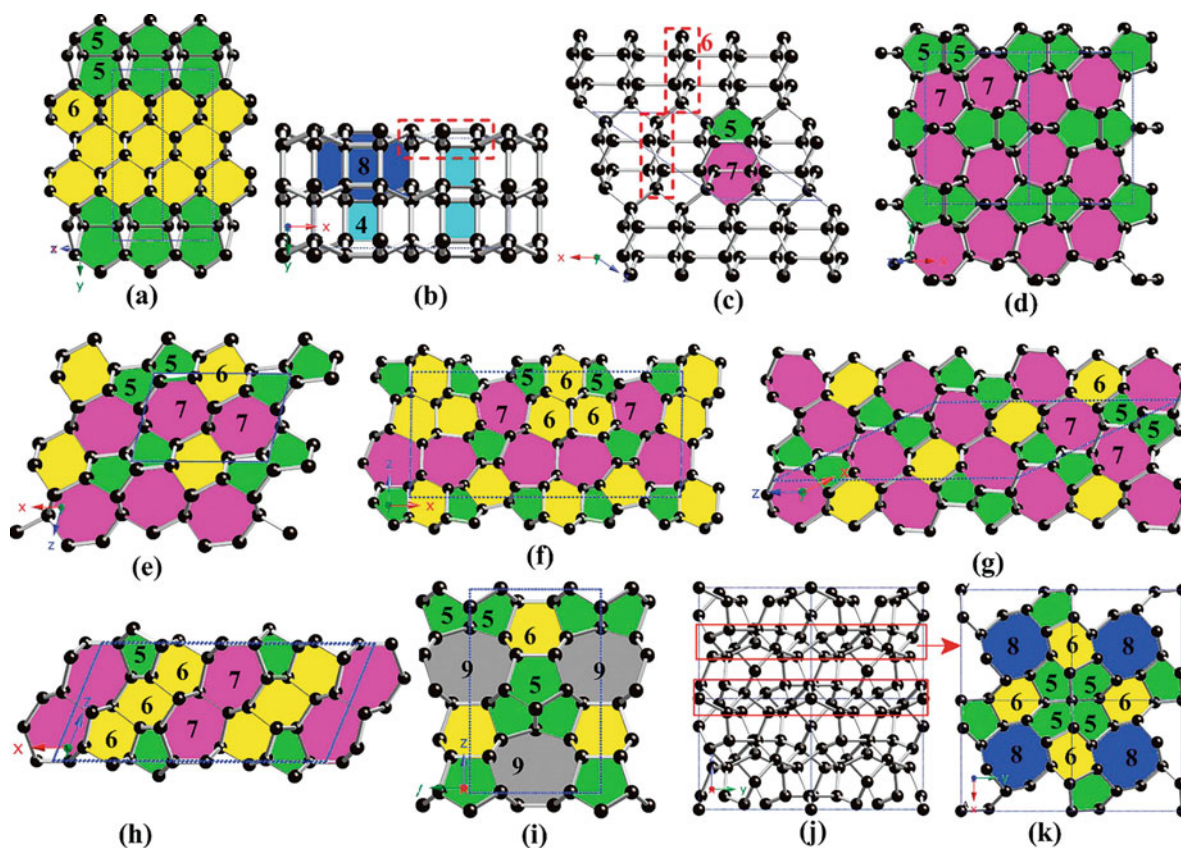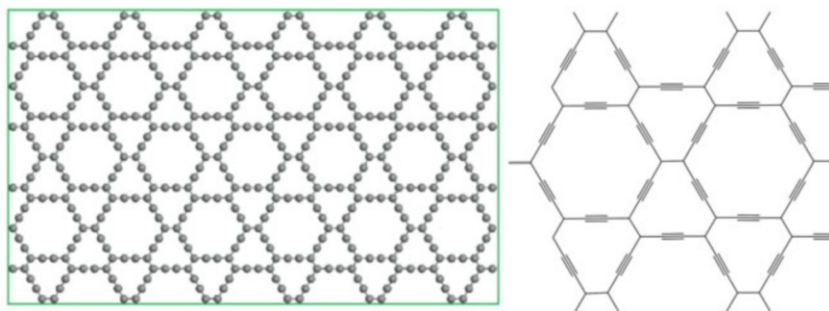
Fig. 6.1 The newly predicted superhard structures of carbon: (**a**) $P222_1$, (**b**) *Imma*, (**c**) *C2/m*-16, (**d**) *Cm*-32, (**e**) $P2_1/m$, (**f**) *Cm*-40, (**g**) *C2/m*-20, (**h**) *C2/m*-28, (**i**) *Amm*2, and (**j**) *I*-4, respectively. The circled atoms in (**j**) are the wrinkled 5 + 6 + 8 member rings, as shown in (**k**). The dished lines in (**b**) and (**c**) indicate the wrinkled six member rings [15]. (Reproduced with permission of the *AIP Publishing Co.*)

6.1   Graphyne

Graphyne [16] is a theorized allotrope of carbon, whose existence was conjectured before 1960 and confirmed by DFT calculations. It has not yet been synthesized in large quantities, although research is continuing, and will be needed to provide experimental data against which to test the computational predictions as well as to clarify some discrepancies regarding mechanical properties. Graphyne was first proposed in 1987 by Baughman et al. as part of a larger investigation into the properties of new forms of carbon that had been sporadically reported, but not systematically investigated.

Graphyne is a variation of graphene that has acetylenic linkages connecting the hexagons of graphene. The proposed structures of graphyne are derived from insertion of acetylene bonds in place of C-C single bonds in a graphene lattice (simply replacing one-third of the C-C bonds in graphene by triple-bonded -C ≡ C- linkages, Fig. 6.2).
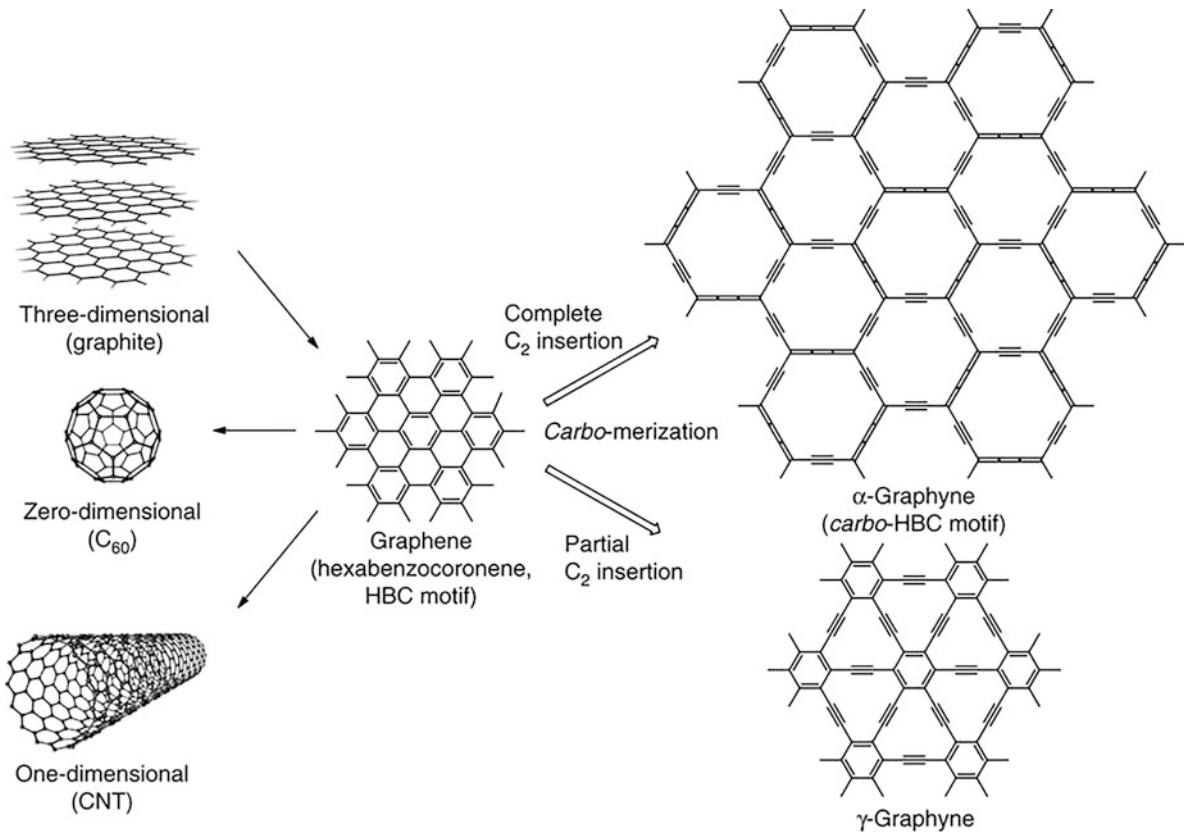
Fig. 6.2 Examples of carbon allotrope materials, from graphene to graphyne and other carbon allotropes [17]. (Reproduced with permission of *Nature*)
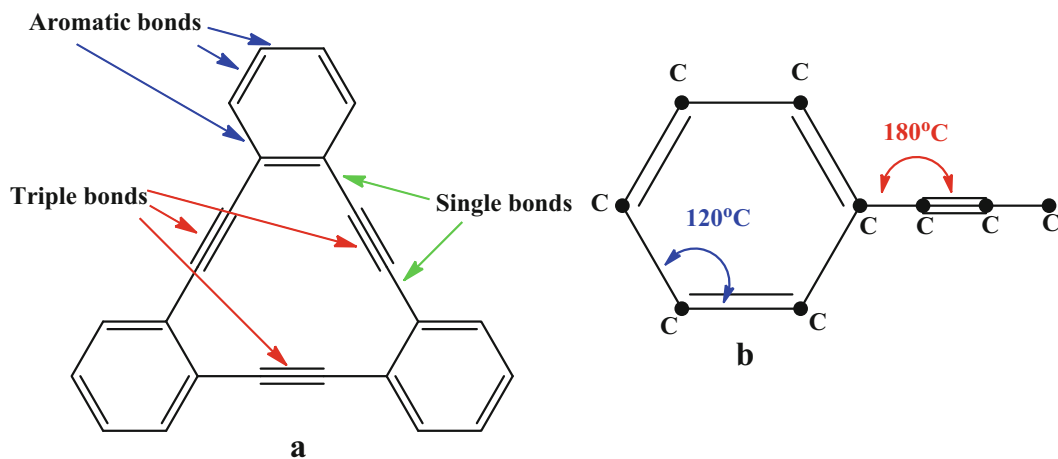

Fig. 6.3 Graphyne cells with (**a**) different interatomic bonds and (**b**) bond angles. (Reproduced with permission of *Hindawi*. Reproduced from: *Journal of Nanomaterials*, 2016, *Volume 2016*, Article ID 7487049, 15 pp.)

Main features of graphyne are as follows:

– It can be considered as a lattice of benzene rings connected by triple bonds. Bonding in graphyne cell is shown in Fig. 6.3.
– It is similar to graphene, since it is also a 2D structure of carbon.
– There are many types of graphynes – as their 2D framework contains triple bonds and not just double bonds as in graphene. According to [18], seven basic structural modifications of graphyne can theorically exist: α-, β1-, β2-, β3-, γ1-, γ2-, and γ3-graphyne.
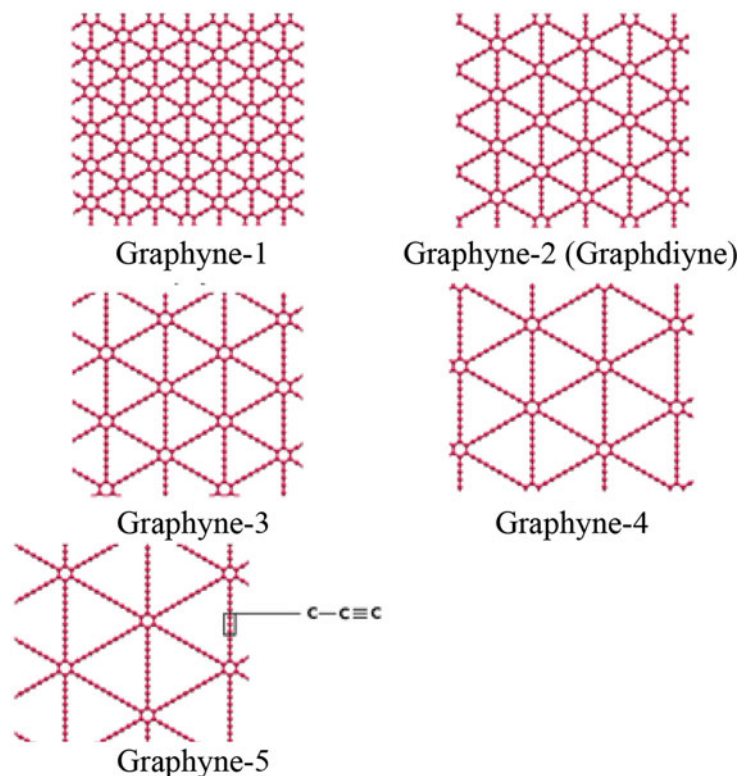
Fig. 6.4 Graphyne, graphdiyne, graphyne-3, graphyne-4, and graphyne-5

– γ-Graphynes should be the most stable structural modifications of graphyne.
– Mixed hybridization sp^n ($1 < n < 2$), in a difference with graphene (sp^2) or diamond (sp^3).
– The presence of sp- and sp^2-hybridized carbon atoms in graphyne causes distinct properties, including large surface area, chemical stability, and electrical conductivity, in addition to the remarkable properties of graphene.
– It can exist in several different geometries, including a hexagonal lattice structure and a rectangular lattice structure.
– Graphyne-like BN sheets can also exist [19].

Graphyne, graphdiyne, graphyne-3, graphyne-4, and graphyne-5 (Fig. 6.4) are allotropes of carbon, all belonging to a family called graphyne-N. These structures are planar sheets of sp and sp^2 bonds of carbon atoms arranged in a crystal lattice. The main difference between these types of graphyne is the number of acetylenic links existing between the hexagonal lattices of carbon atoms (Fig. 6.5). Graphyne-N has 33% of the C-C bonds of graphene replaced by one acetylenic unit. Although having a fixed amount of C-C bonds, there are several structures of graphyne. The most known are α-, β-, γ-, and R-graphyne and 6,6,12-graphyne (Fig. 6.6). Four other 2D p-metallic carbon allotropes, it is also known about possible existence of hexagonal ones (C_{65}-, C_{63}-, and C_{31}-sheets) and one tetragonal one (C_{41}-sheet) [20]. The C_{65}-, C_{63}-, and C_{41}-sheets are more stable, and the C_{31}-sheet is slightly less stable than graphyne.

Graphdiyne (it is part of the graphyne family; however, due to its interesting properties, it is typically considered separately) is a variant of graphyne that contains two acetylenic linkages in each unit cell rather than the one linkage as in graphyne. As a result, graphdiyne does not share graphyne's exceptional mechanical properties. Graphdiyne is a softer material than either graphyne or graphene, with an in plane stiffness of 120 N/m, which is equivalent to a Young's modulus of 375 GPa, if a thickness of 0.320 nm is assumed. Graphdiyne was first predicted by Haley et al. in 1997. Main features of graphdiyne are as follows:

– It was synthesized on Cu and Ag surfaces.
– It exhibits a nanoweb-like structure characterized by triangular and regularly distributed pores, which form a nanoporous membrane.

A 2D carbon allotrope, *rectangular graphyne* (R-graphyne, Figs. 6.6, 6.7, and 6.8) with tetra-rings and acetylenic linkages, was proposed [22] by first-principles calculations, showing that it is metallic as the valence band crosses the Fermi level. Among other results, the most intriguing feature is that bandgaps of R-graphyne nanoribbons oscillate between semiconductor

Graphyne

Graphdiyne
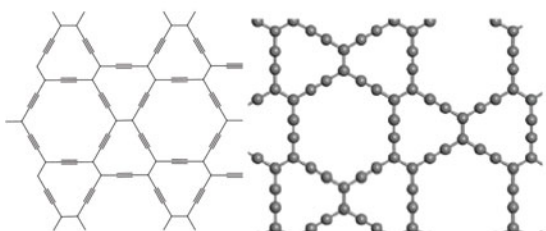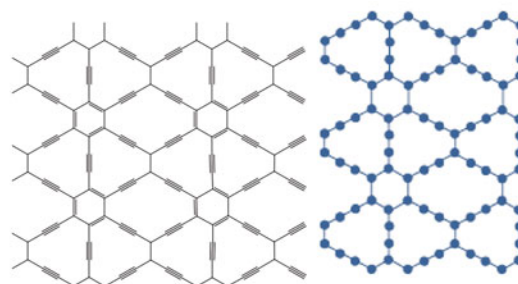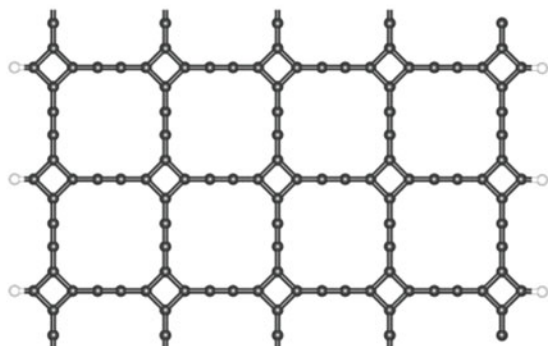
Graphyne-3
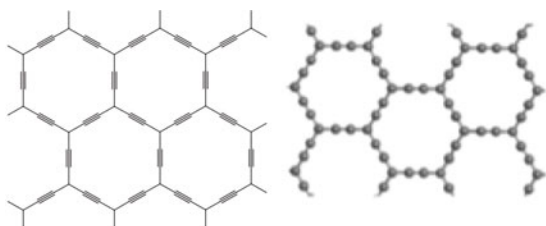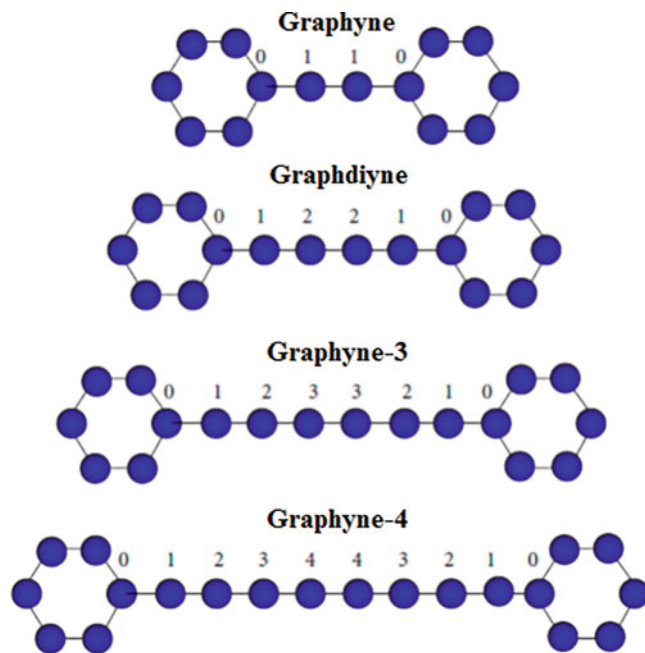
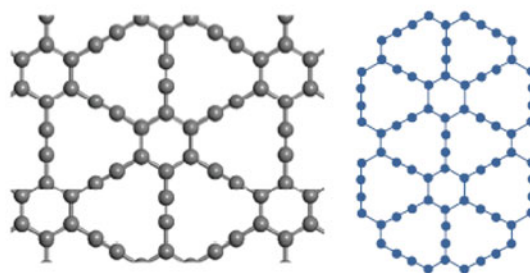**Graphyne-4**
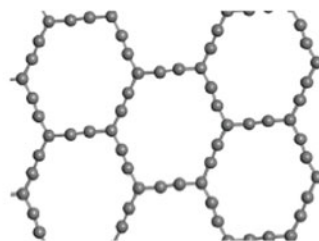
α-Graphyne

α-Graphyne under a shear strain

β-Graphyne

6,6,12-Graphyne

R-graphyne

γ-Graphyne[21‡]

Fig. 6.6 α-, β-, γ-, and R-graphyne and 6,6,12-graphyne [21]. (Reproduced with permission of *Springer*)

Fig. 6.7 The configurations of R-graphyne nanoribbons obtained by cutting through an infinite R-graphyne along two directions. (**a**) Armchair nanoribbons of R-graphyne with widths $N_A = 1$, 2 and 5, where N_A denotes the number of chains of tetra carbon rings. (**b**) Zigzag edged R-graphyne nanoribbons with widths $N_Z = 1$, 1.5, and 3.5 expressed by N_Z. The black and white balls represent carbon and hydrogen atoms, respectively. (Reproduced with permission of the *Royal Society of Chemistry*)
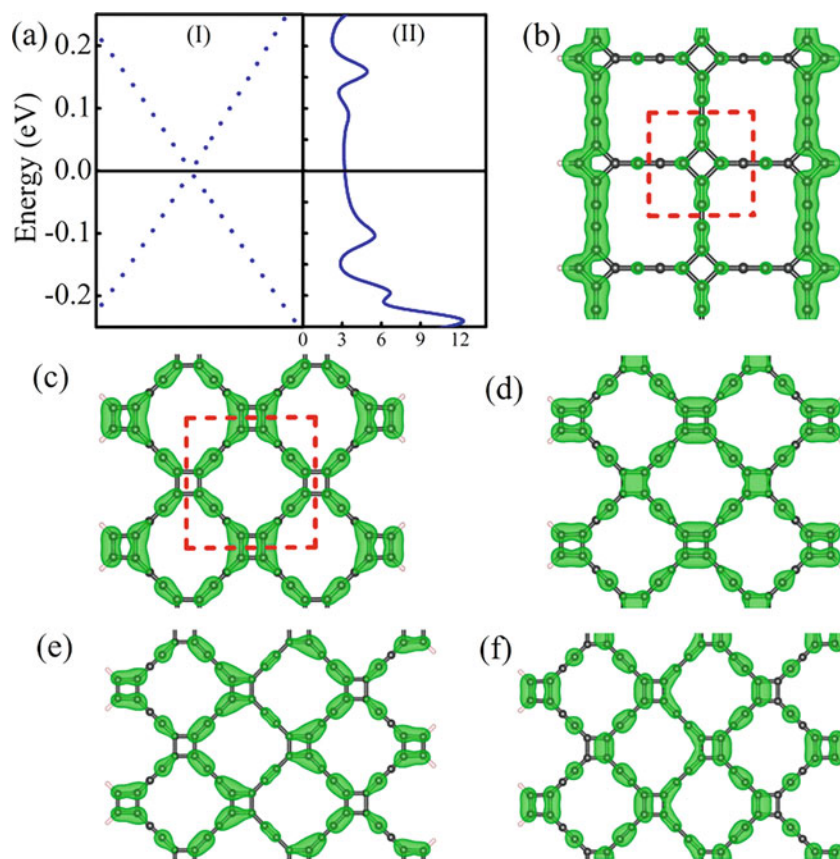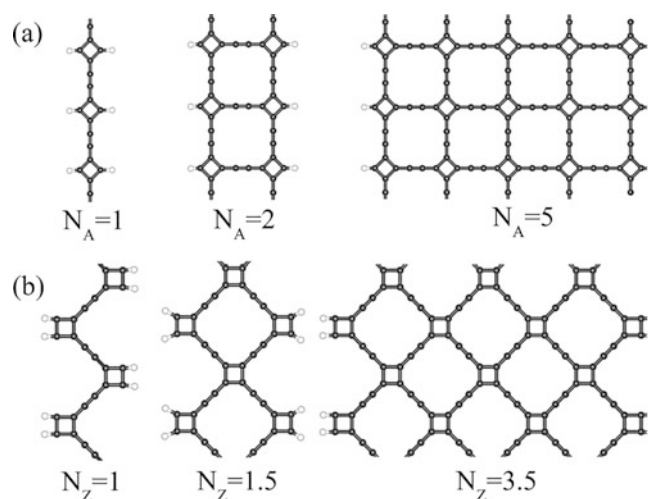
Fig. 6.8 The electronic structures and charge-density distribution of R-graphyne nanoribbons. (**a**) Amplification of the band structure(I) and DOS (II) around the meeting point for $N_Z = 2.5$. The charge-density distribution near EF for armchair R-graphyne nanoribbons ($N_Z = 3$). (**b**) The maximum point at valence band (**c**)/(**e**) and the minimum point at conduction band (**d**)/(**f**) for $N_Z = 2.5$/$N_Z = 3$. The black balls represent carbon atoms. (Reproduced with permission of the *Royal Society of Chemistry*)

and metallic states as a function of width. Particularly, the zigzag edge nanoribbons with half-integer repeating unit cell exhibit unexpected Dirac-like fermions in the band structures.

Certain attention is paid to graphyne scrolls and ribbons, since graphyne could exist not only in the plane form but also in scroll-like structure. Thus, the formation of graphyne and graphdiyne nanoscrolls, structures obtained by rolling up graphyne

sheets into papyrus-like structures, was calculated [23] for a series of graphyne (α-, β-, and δ-types) structures, as well as their thermal stability for a temperature range of 200–1000 K. Their stability was found to be dependent on a critical value of the ratio between length and height of the graphyne sheets. Additionally, these structures are structurally less stable then graphene-based nanoscrolls, which were explained by the graphyne higher structural porosity which results in a decreased π-π-stacking interactions. The intrinsic electronic and transport properties of four distinct polymorphs of graphyne (α-, β-, γ-, and 6,6,12-graphynes) and their nanoribbons (GyNRs) were studied using DFT coupled with the non-equilibrium Green's function (NEGF) method [24]. Their nanoribbons possess many electronic, magnetic, and transport properties that are notably different from those of known graphene and BN nanoribbons. Among the four graphyne sheets, 6,6,12-graphyne displayed notable directional anisotropy in the transport properties. In a related report [25], it was shown that all graphyne and graphdiyne nanoribbons with armchair and zigzag edges are semiconductors (with bandgaps of 0.59–1.25 eV armchair, 0.75–1.32 eV zigzag for graphyne nanoribbons, and of 0.54–0.97 eV armchair, 0.73–1.65 eV zigzag for graphdiyne nanoribbons) with suitable bandgaps similar to silicon and their bandgaps decrease as widths of nanoribbons increase.

Several other properties of graphynes have also been DFT-calculated. Thus, the *mechanical properties* of graphyne sheets were evaluated by full atomistic first-principles-based ReaxFF molecular dynamics [26]. It was established that, unlike graphene, (a) the fracture strain and stress of graphyne depends strongly on the direction of the applied strain and the alignment with carbon triple-bond linkages, ranging from 48.2 to 107.5 GPa with ultimate strains of 8.2–13.2%; (b) the sparser carbon arrangement in graphyne combined with the directional dependence on the acetylenic groups results in internal stiffening dependent on the direction of applied loading, leading to a nonlinear stress–strain behavior. In case of metal-decorated graphyne, the mechanical properties of Na- and Pt-decorated arrays of graphyne sheet were DFT-investigated [27]. The proposed structures were consisted of Na- and Pt-decorated graphyne sheet (CC), analogous system of boron nitride sheet (BN-yne), and graphyne-like BN sheet (CC-BN-yne). The largest value was presented by CC, which was higher than that of obtained from non-decorated systems. The *elastic properties* of graphyne (Young's modulus, Poisson's ratio, bulk modulus, and shear modulus) were established [28], and an analytical molecular mechanics model was proposed for relating the elastic properties of graphynes to their atomic structures directly [29]. *Thermal conductance* of β-graphyne is only approximately 26% of that of the graphene counterpart and also shows evident anisotropy [30].

Various forms of graphynes have been studied in respect of their interaction with metal and nonmetal surfaces, in particular possible formation of graphyne (α-, β-, and γ-phases) on transition-metal surfaces (Ru(0001), Rh(111), and Pd(111), Fig. 6.9) [31]. The interlayer binding between graphynes and the metal substrates was found to reduce the formation energies of graphynes by 0.16–0.34 eV, such that the growth of graphynes is competitive to that of graphene on the metal surfaces. The α-phase of graphyne is thermodynamically most favorable in the carbon-poor environment, while formation of graphene is dominant in the carbon-rich condition. Similar studies, related more with carbyne than graphyne, on the electronic and geometric structures of carbyne on transition-metal surfaces were also investigated by theoretical calculations [32]. It was found that carbyne on non-active metal surfaces (Cu) has a polyynic structure, while a polycumulenic structure is more stable on active catalyst surfaces (Ni, Rh, Ru) (Figs. 6.10 and 6.11). Carbyne with a size of N < 10–13 is predicted to be the ground state of carbon clusters on various transition-metal surfaces. Beyond the critical size of 10–12, the carbyne structure becomes
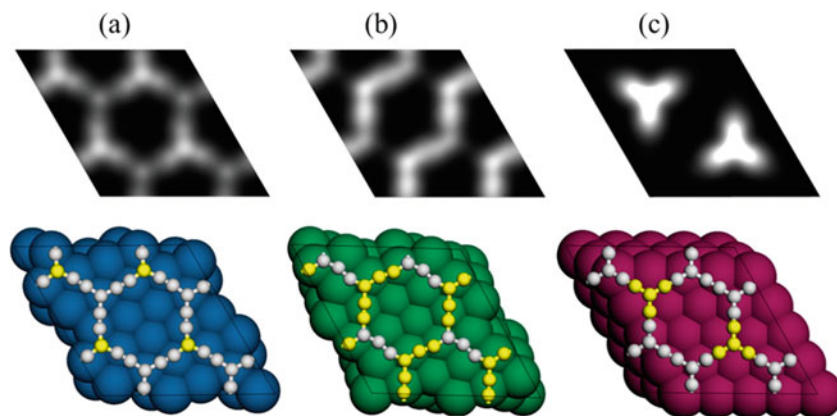
Fig. 6.9 Simulated STM images of α-graphyne on (**a**) Ru(0001), (**b**) Rh(111), and (**c**) Pd(111), respectively, using a bias voltage of −2 V. The top views of the atomic structures of α-GY on the three metal substrates are shown below each STM image. The C, Ru, Rh, and Pd atoms are indicated in silver, blue, green, and wine, respectively. The yellow balls indicate the C atoms, which are buckled up in the out-of-plane direction and hence show larger brightness in the STM images. (Reproduced with permission of the *American Chemical Society*)

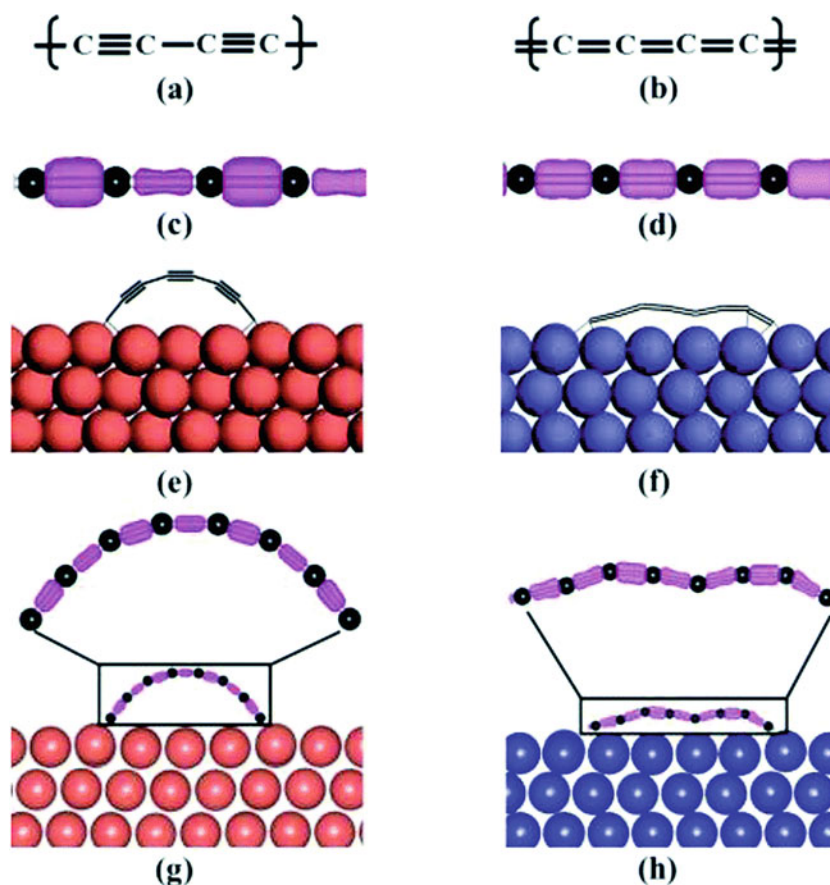**Fig. 6.10** The polyyinc carbyne formation with alternative single and triple bonds (–C ≡ C–)$_n$ (**a**) and the polycumulenic carbyne with double bonding (=C=C=)$_n$ (**b**); the electron densities of polyyinc carbyne (**c**) and polycumulenic carbyne (**d**); the formation of a carbon chain with 8 carbon atoms on the Cu(111) surface (**e**) and Ru(0001) (**f**) surfaces and their corresponding electron densities (**g**, **h**). (Reproduced with permission of the *Royal Society of Chemistry*)

less stable than the sp^2 carbon network. The polyyinc carbyne tends to be curved up on the less active metal surface, while polycumulenic carbyne prefers to be formed in a straight line on the active metal surface. The self-assembly of carbyne on a metal substrate could lead to the synthesis of graphyne (Fig. 6.12). In addition, atomic, electronic, and quantum transport properties of γ-graphyne absorbed on the silicon (111) surface were investigated from atomistic first principles [33]. The most interesting result is that the transmission spectra of the γ-graphyne/Si(111) hybrid device has a high broad peak at the Fermi level due to a combination of states on γ-graphyne/Si(111), and this peak persists even for the trenched γ-graphyne/Si(111) systems where the Si is removed underneath the γ-graphyne in the scattering region.

Although graphyne has yet to be synthesized well, its properties are promising for several applications, such as nanofillers, transistors, sensors for inorganic and organic substances, semiconductor metal hybrids, anisotropic conductors, and desalinators, among others. Thus, a nanoscale capacitor composed of heterostructures derived from finite size graphyne flake and graphene (nitride) flake (graphyne/graphene, graphyne/h-BN, graphyne/AlN, graphyne/GaN) was proposed and DFT studied [34], taking into account a significant charge transfer between two flakes generates permanent dipole in this heterostructures. The formation process of these heterostructures was found to be exothermic and comparable with the binding energy of graphene bilayer. The charge stored by each flake, energy storage, and capacitance are switchable under external electric field. These structures can be considered as a suitable template for charge and energy storage.

The adsorption of sulfur dioxide (SO_2) on pristine and modified graphyne (with defects and adatoms) was investigated by DFT calculations [35], showing changes according to the dopant atom, site of doping, and vacancy. These changes were especially strong in case of boron doping at the sp-hybridized carbon site and introducing a single carbon atom vacancy, causing deformation of the graphyne structure and electron redistribution. It was established that these graphynes are a potential material for SO_2 gas sensors. Similarly, the adsorption of formaldehyde on graphyne was investigated to search high sensitivity sensors for detection of formaldehyde [36]. It is found that formaldehyde is physisorbed on the graphyne (and also
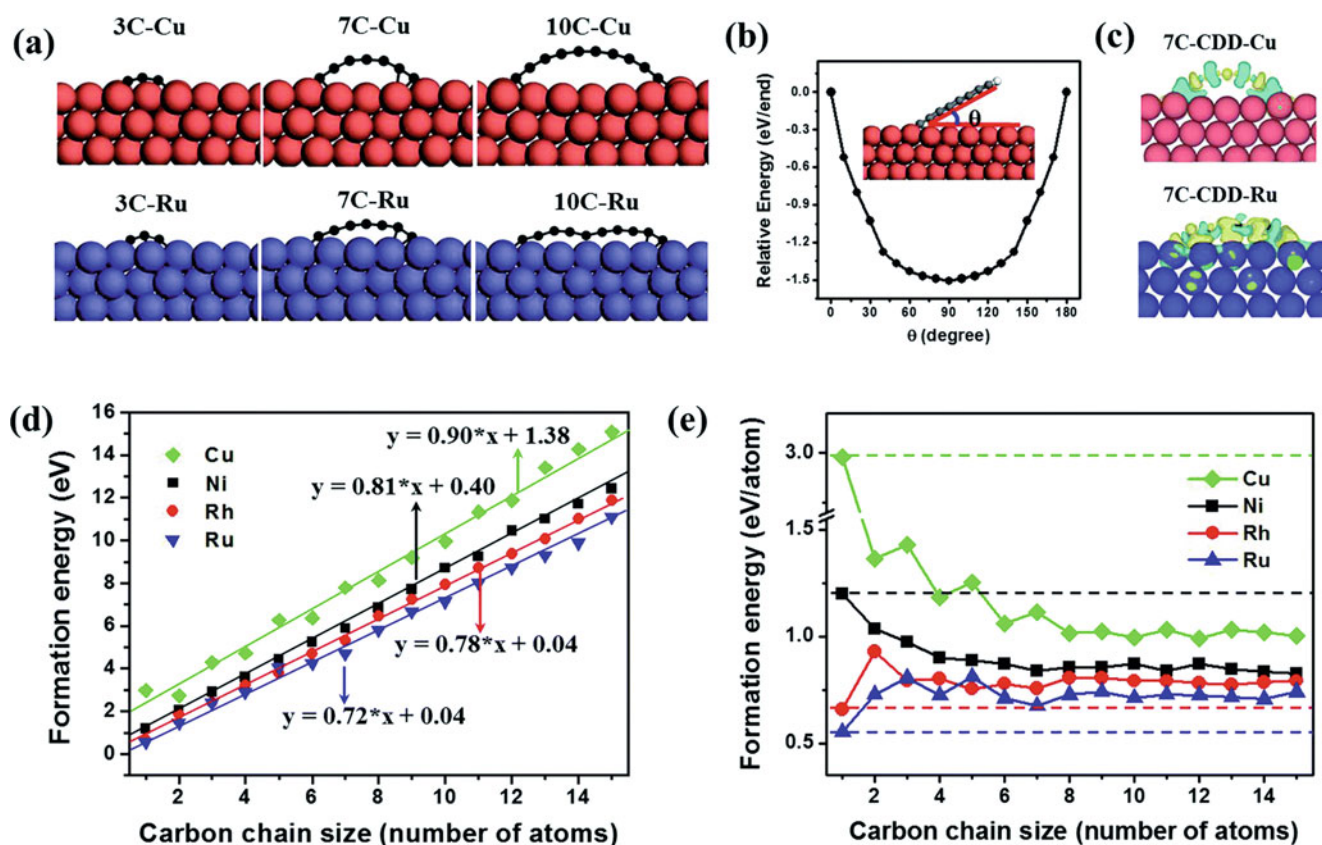
Fig. 6.11 (**a**) Selected structures of carbon chains (C3, C7, C13) on Cu(111) and Ru(0001) surfaces. (**b**) The relative binding energy of a carbyne on the Cu(111) surface as a function of the tilt angle, θ. (**c**) Charge-density difference (CDD) for carbon chains with seven carbon atoms on Cu(111) and Ru(0001) surfaces. (**d**) Formation energies of carbyne/carbon chains (1C–15C) on Cu, Rh, Ru, and Ni surfaces, respectively. All the energies are fitted by the inserted linear equations. (**e**) Formation energies per carbon atom of carbon chains on Cu, Rh, Ru, and Ni surfaces. (Reproduced with permission of the *Royal Society of Chemistry*)
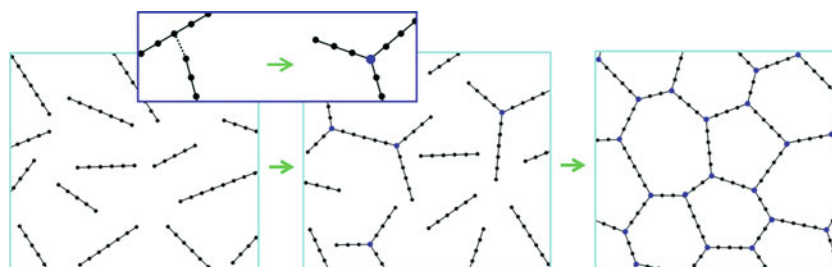

Fig. 6.12 Illustration of graphyne formation on a transition-metal surface by the self-assembly of the carbyne chains. (Reproduced with permission of the *Royal Society of Chemistry*)

on graphene) with large binding distance, small binding energy, and small charge transfer, modifying the electronic properties of semimetallic graphene, α-graphyne, and β-graphyne and semiconducting γ-graphyne. HCOH prefers to orient perpendicularly with H atoms close to the sheets (Fig. 6.13). Also, adsorption of polycyclic aromatic hydrocarbons (PAHs) onto graphyne was calculated [37], showing that, due to the porous character of graphyne, the adsorption strength of PAHs onto graphyne surfaces is expected to be lower with respect to graphene (a perfect π-extended system).
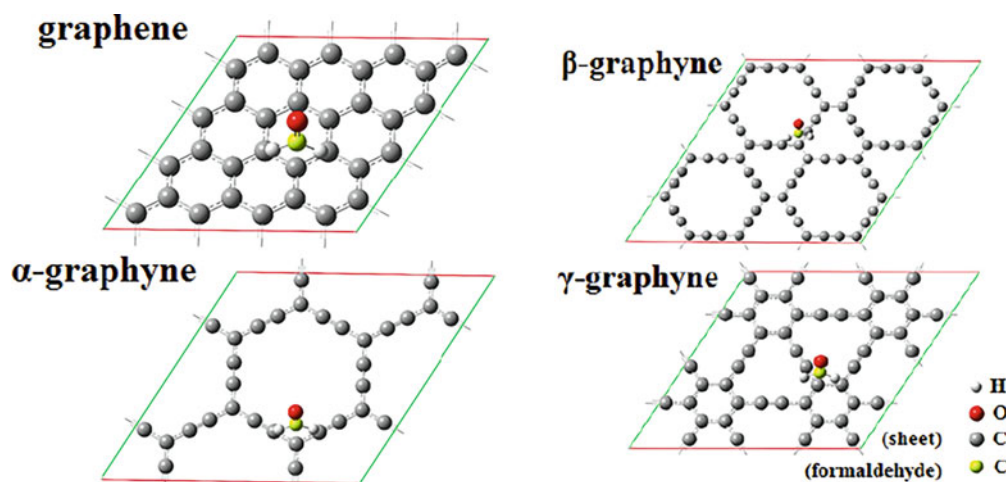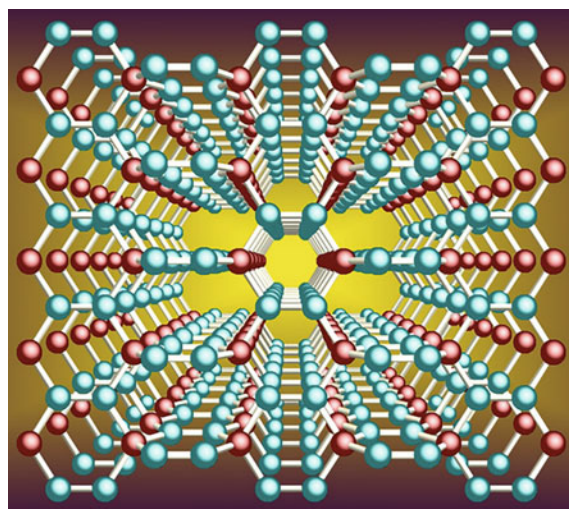
Fig. 6.13 Adsorption configurations of formaldehyde on graphene, α-graphyne, β-graphyne, and γ-graphyne. (Reproduced with permission of the *Elsevier Science*)

6.2   Metallic Carbon[1,2]

One of the unsolved issues in carbon science has been to find a 3D form of carbon that is metallic under ambient conditions. Carbon has abundant allotropes with superhardness, but few of them are metallic. Some rare carbon structures seem to be metallic (for instance, armchair carbon nanotube [38, 39] in 1D systems or 2D graphene sheet) or were proved to be nonmetallic (dense cold compressed graphite, T-, L-, Y-carbon, and cubane-based porous carbon). DFT studies are widely used for prediction of possible metallic carbon allotropes and evaluation of their stabilities and magnetic properties. Thus, for example, carbon nanostructures with unusually large paramagnetic moments were discovered [40] in a theoretical study of the electronic and magnetic properties of carbon nanotubes bent into toroids (see the section above on *carbon nanotori*). The large paramagnetic moment is due to the interplay between the toroidal geometry and the ballistic motion of the π electrons in the metallic nanotube.

Metallic carbon has been extensively studied for its potential applications in superconductivity, catalysis, and electronic devices. Currently, the design of metallic carbon is mainly by educated intuition which could miss some more stable

---

[1]This term does not deal with carbon nanotubes containing metals as impurities.

[2]Reproduced with permission of the PNAS (*Proc. Natl. Acad. Sci. USA*. 2013, *110*(47), 18809–18813).

allotropes. Metallic carbon structures can possess properties even more novel than the semiconducting carbon structures, possessing the following features:

– Exhibits phonon–plasmon coupling and displays negative differential resistance and superconductivity.
– Highly efficient catalytic property is possible due to its high electronic density of states (DOS) at the Fermi level.
– Metallic carbon can become magnetic when the stoner-like criterion is satisfied.
– Metallic carbon, due to its high density of states (DOS) at the Fermi level, can be effective as a catalyst.
– Metallic carbon showed a number of intriguing properties such as phonon-plasmon coupling, superconductivity, and negative differential resistance.
– Metallic 3D carbon at this point does not exist: this is only theoretically predicted (see below). Some hypothetical metallic 3D carbon allotropes such as $ThSi_2$-type tetragonal carbon, hexagonal H-6 carbon, and K4 carbon were found to be dynamically unstable.

Some recent studies by first-principles calculations have revealed possibilities of existence of several metallic carbon allotropes at distinct conditions. Thus, a stable anisotropic metallic carbon allotrope (Hex-C_{24}, Fig. 6.14) phase with superhardness was proposed by DFT calculations [41]. The Hex-C_{24} can be thought of as a superlattice of carbon nanotubes and graphene nanoribbons composed of sp^2- and sp^3-hybridized carbon atoms. An evaluated possible synthetic route (Fig. 6.15) toward Hex-C_{24} from graphyne multilayers indicated to a uniaxial pressure of around 25 GPa, with the energy
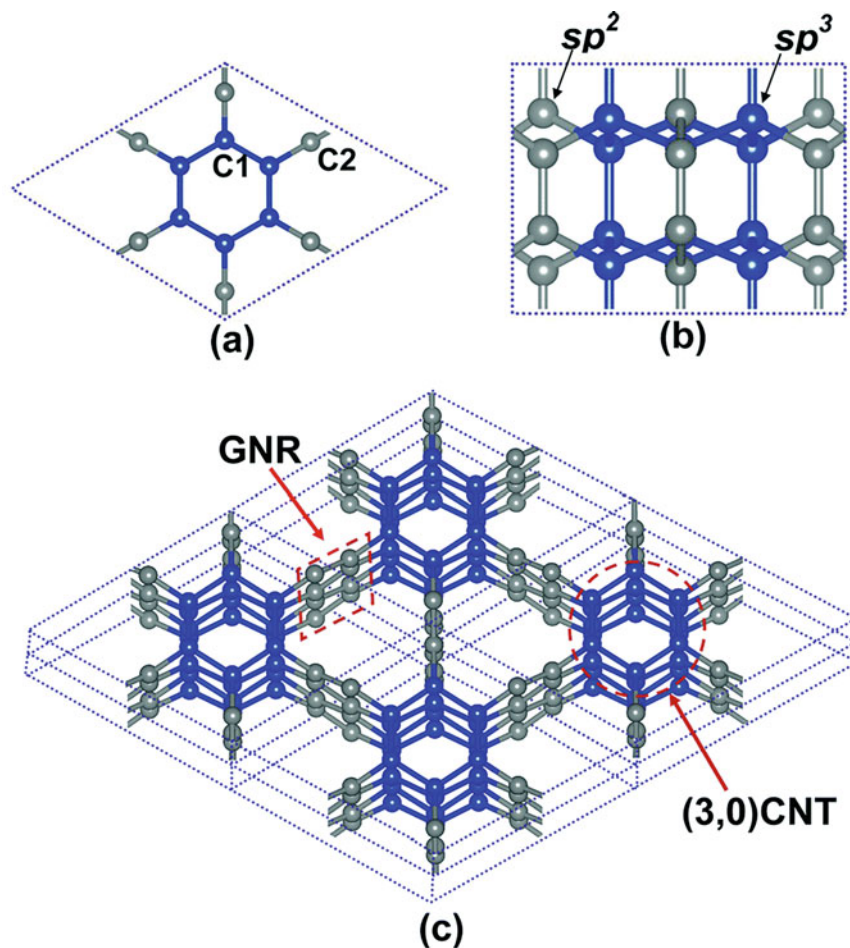
Fig. 6.14 Atomic structure of Hex-C_{24} composed of sp^2- and sp^3-hybridized carbon atoms. (**a**) Top view, (**b**) side view, and (**c**) schematic representation of the superlattice of (3, 0) CNTs and GNRs. (Reproduced with permission of the *Royal Society of Chemistry*)
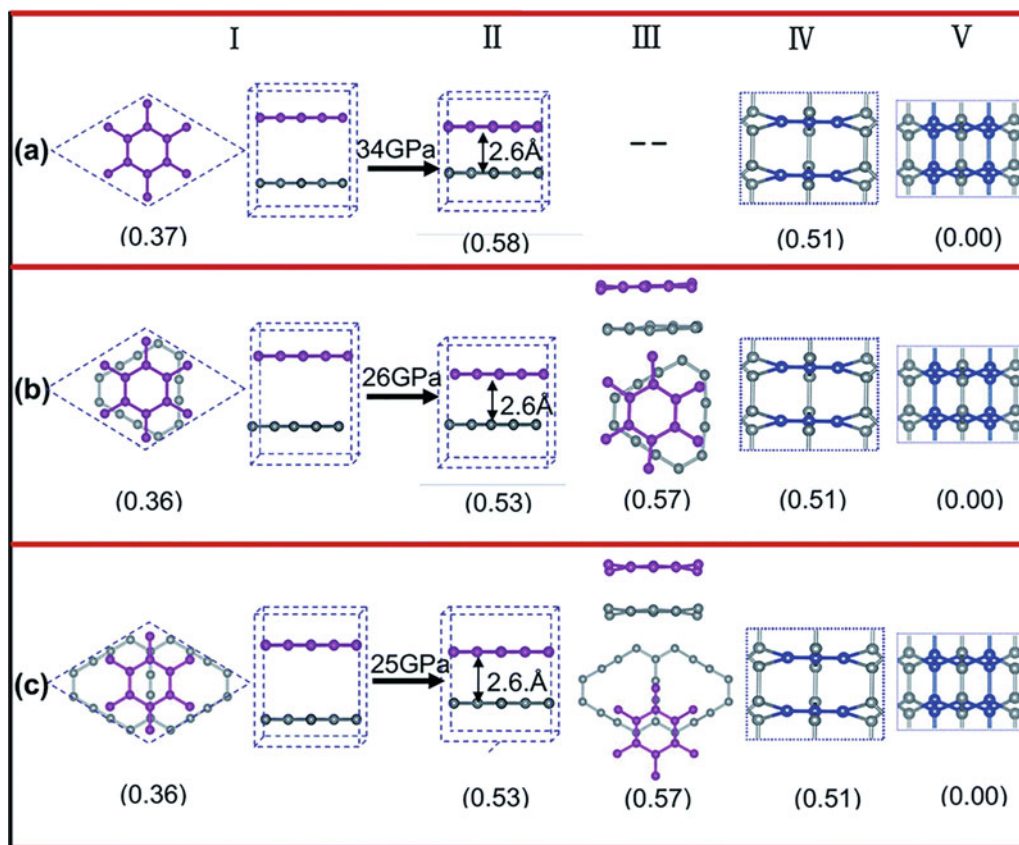
Fig. 6.15 A possible pathway of the structural transition of graphyne to Hex-C_{24}. The energy of the product (Hex-C_{24}) is set to zero, and the numbers in parentheses are the energy referenced to the product (eV per atom). I (reactant), II (critical state), III (TS), IV (intermediate), and V (product) columns show the key states in the reaction process. (**a**), (**b**), and (**c**) rows show the transition processes of α, β_1, and β_3 structures. (Reproduced with permission of the *Royal Society of Chemistry*)

barrier of this endothermic transition to be 0.04 eV per atom, while at a pressure of 34 GPa, the transition is barrierless for specific initial configurations. A 3D metallic carbon (Tri-C_9, Fig. 6.16) was built by distorting the sp^3 hybridization bond [42]. The Tri-C_9 is a metastable metallic carbon with a considerable bulk modulus of 365 GPa and that the metallic behavior of Tri-C_9 originates from the π bonds near Fermi level. A feasible synthesis route for Tri-C_9 was proposed by compressing graphite.

The theoretical existence of a 3D form of carbon, that is, metallic *under ambient conditions and pressure*, was predicted that it is formed from interlocking hexagons, dynamically, mechanically, and being thermally stable, and may be synthesized chemically by using benzene or polyacenes molecules, unlike high-pressure techniques that require 3 TPa to make metallic carbon [43]. It was demonstrated that 3D carbon structures formed of interlocking hexagons are metallic under ambient conditions; they are systems with hybridized sp^3 and sp^2 bonding. The sp^3-bonded carbon atoms guarantee their stability, and the sp^2-bonded carbon atoms ensure their metallicity. At 500 K, the metallic T6 phase (Fig. 6.17) changes to the T12 phase, whereas the metallic T14 phase changes to the metallic T28 phase. The predicted metallic carbon could have potential applications ranging from electronics and superconductivity to lightweight space materials.

A 3D metallic carbon phase, termed Hex-C_{18} (Fig. 6.18), also composed of sp^2- and sp^3-hybridized carbon atoms, was found [44] to be energetically more favorable than most of the previously identified 3D metallic carbon allotropes. It was DFT-predicted that Hex-C_{18} not only possesses a high thermodynamic stability, large heat capacity, high Debye stiffness, anisotropic elasticity, and super hardness but also is a promising anode material for lithium-ion batteries. Another stable
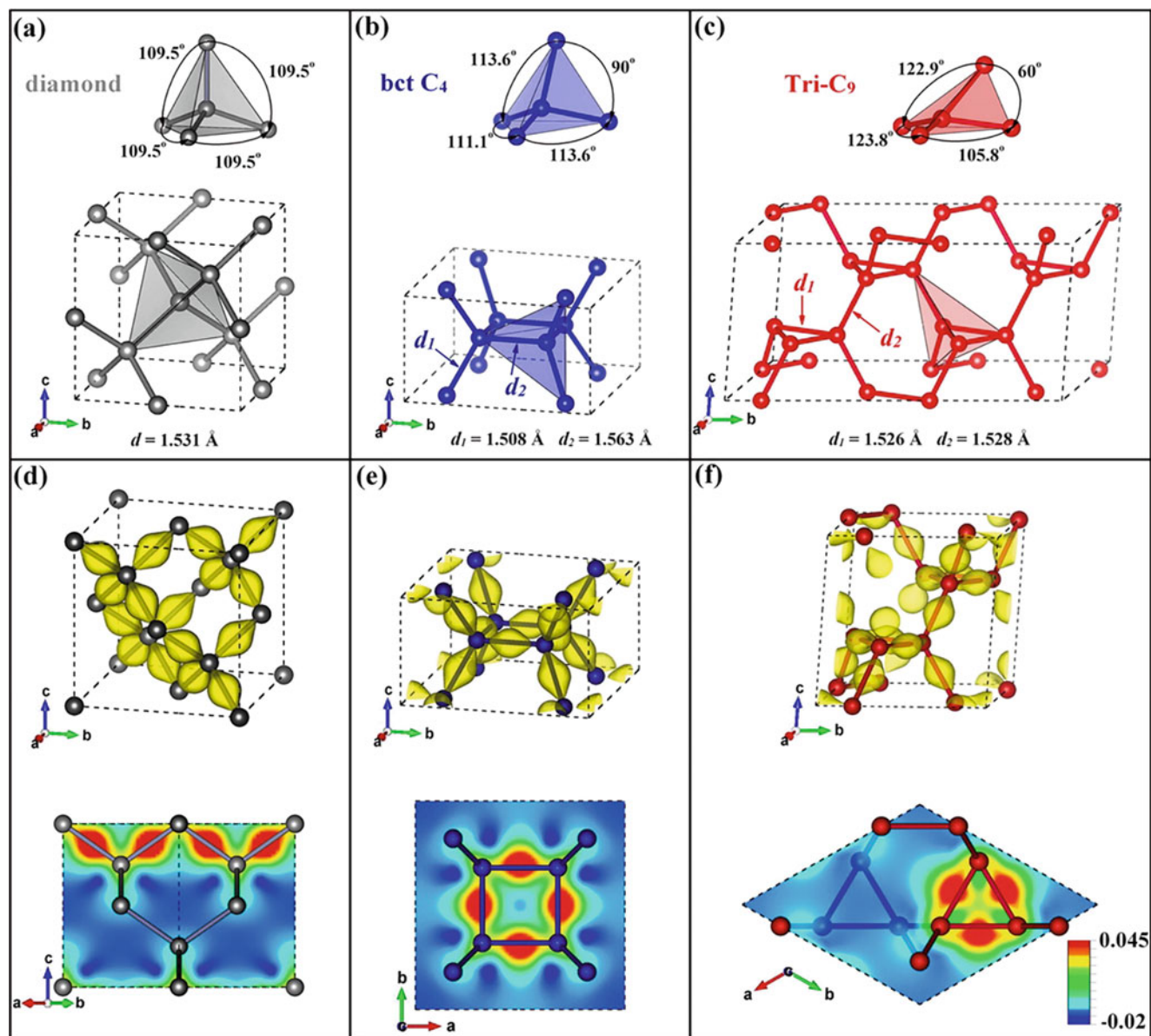
Fig. 6.16 (**a–c**) Building block (top) and corresponding crystal structure (bottom) for diamond, bct C_4, and Tri-C_9 ($1 \times 2 \times 1$ supercell), respectively. (**d–f**) Bonding charge density (top) and its 2D slices (bottom) for diamond, bct C_4, and Tri-C_9, respectively. The bonding charge density is the difference between the total charge density of the structure and the superposition of the charge density of the neutral constituent atoms. The isosurface of the bonding charge density is 0.2 e/Å^3. The red and blue colors in the slices indicate the electron accumulation and depletion, respectively. (Reproduced with permission of the *American Chemical Society*)

metallic carbon allotrope is H_{18} carbon (Fig. 6.19) with a mixed sp^2–sp^3-hybridized bonding network [45]. It would be one of the unidentified carbon phases observed in detonation experiments, and it has a metallic feature mainly due to the C atoms with sp^2 hybridization. This phase is composed of 18 atoms per hexagonal primitive cell (hereafter termed H_{18} carbon), having a larger atom density of 3.135 g/cm^3 compared to 2.28 g/cm^3 for graphite. This phase is anticipated to be useful for practical applications such as electronics and mechanics devices.

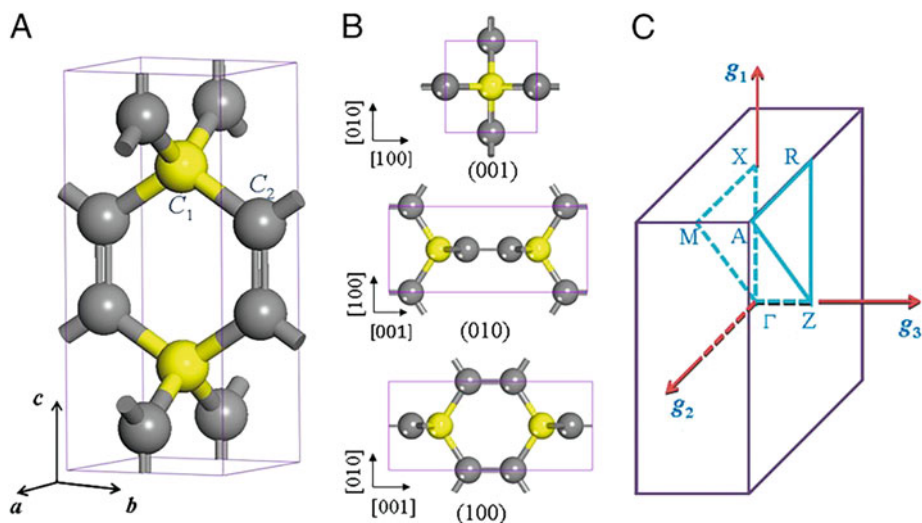**Fig. 6.17** Crystal structure of T6-carbon: (**a**) perspective view and (**b**) polyhedral view from three axial directions. (**c**) Corresponding first Brillouin zone and the high-symmetry K point paths. (Reproduced with permission of the *PNAS*)
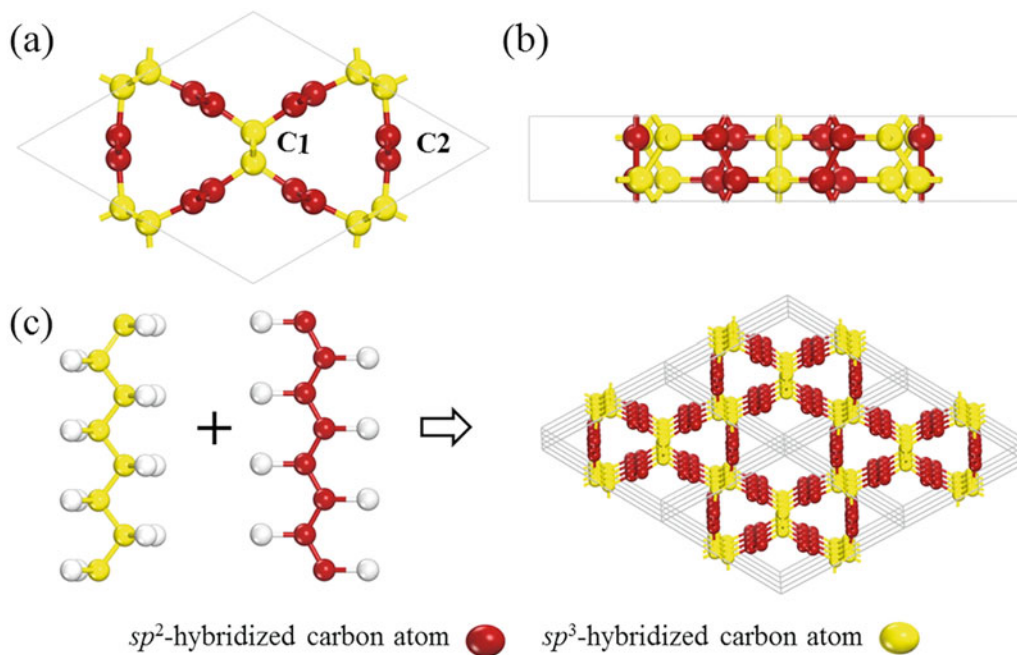

Fig. 6.18 (**a**) Top view and (**b**) side view of the optimized structure of Hex-C_{18}. (**c**) A schematic illustration of a possible synthesis strategy for Hex-C_{18} by using C-H chains via dehydrogenation and assembly. (Reproduced with permission of the *Elsevier Science*)

Fig. 6.19 Top (**a**) and side (**b**) views of H_{18} carbon in *P6/mmm* (D^1_{6h}) symmetry with single and double bonds. (Reproduced with permission of *Nature*)
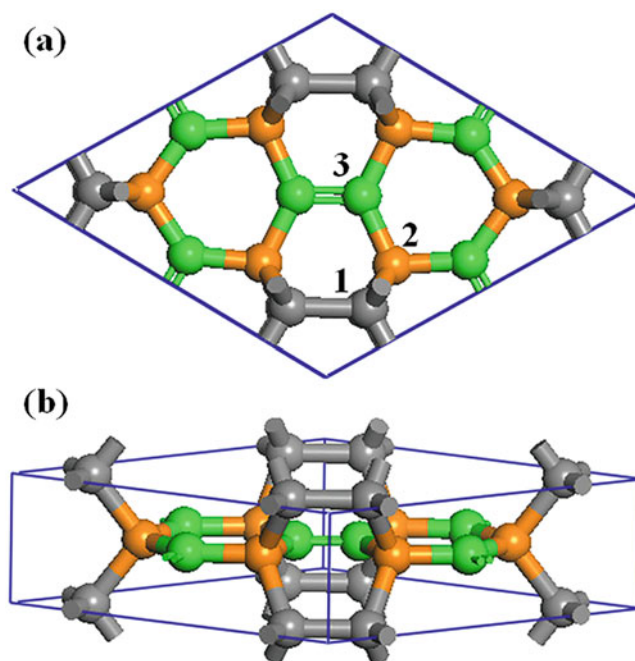
6.3   bcc-Carbons[3] and Other Related Polymorphs
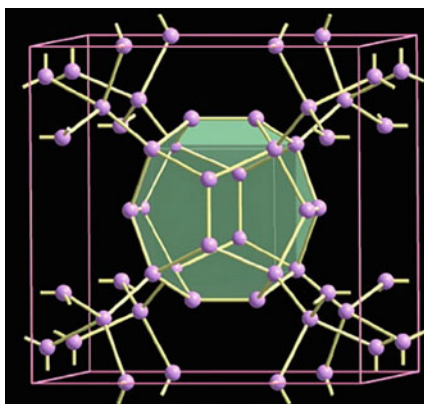
It was predicted that the diamond can be transformed into the so-called C_8 structure (such crystal structures are described in detail in [46]), a body-centered cubic structure (bcc-carbon) with eight atoms in the unit cell at ultrahigh pressures of above 1000 GPa. Some peculiarities of various bcc-carbons, found in available literature, are as follows:

– bcc-Carbon was first predicted in 1989 [47].
– bcc-C_6 has an indirect band gap of 2.5 eV.
– bcc-C_6 is an excellent material for building few-layer structures.
– bcc-C_6 possesses exceptionally low-surface energy.
– Cubic C_8 was predicted to be aromatic (according to Hirsch's rule), but very reactive, both with itself and triplet oxygen [48].
– bcc-Carbon phase might have importance in astrophysics.

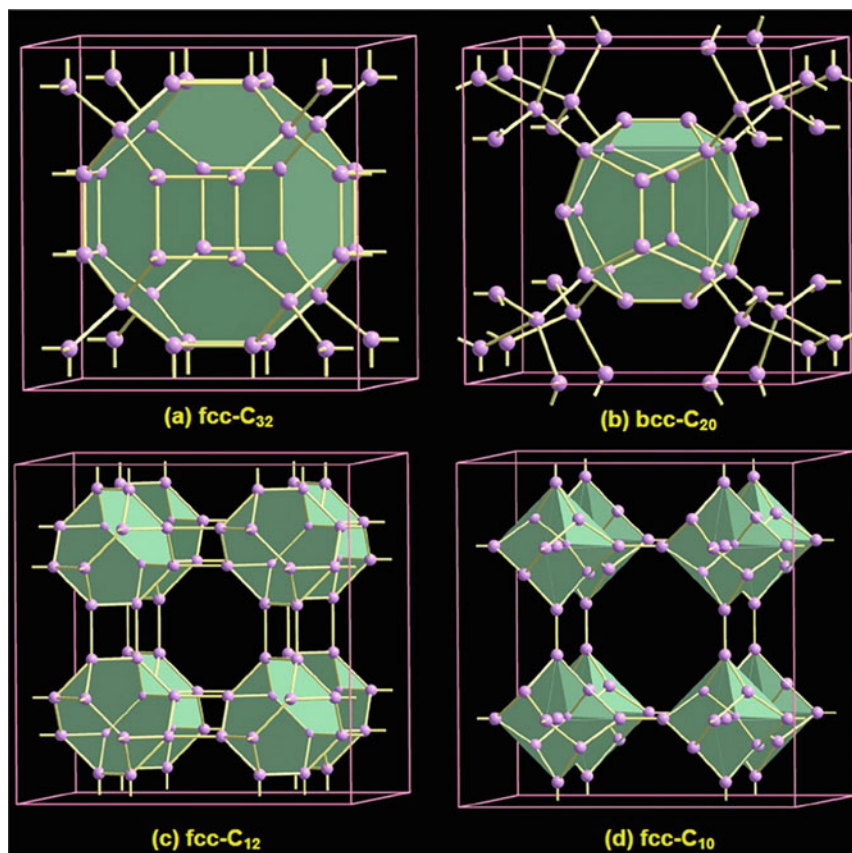[3]Reproduced with permission of the *American Chemical Society* (*J. Phys. Chem. C*, 2012, *116*(45), 24233–24238).

Fig. 6.20 Crystal structures of (**a**) fcc-C_{32}, (**b**) bcc-C_{20}, (**c**) fcc-C_{12}, and (**d**) fcc-C_{10}, respectively. They consist of identical C_{32}, C_{20}, C_{12}, and C_{10} cages, respectively. Notably, a central atom in the C_{10} cage bonds to the nearest four atoms

Among many existing and predicted elemental carbon architectures, a group of 3D allotropes with cubic modifications (fcc-C_{10}, fcc-C_{12}, bcc-C_{20}, and fcc-C_{32}, Fig. 6.20) and with quite low density were proposed by employing an ab initio particle-swarm optimization methodology for crystal structure prediction [49]. Some of them were experimentally synthesized and naturally exist. The lightest fcc-C_{10} has a comparable density to C_{60} fullerene, and the densest fcc-C_{32} has a slightly higher density than graphite. All they are semiconductors with excellent mechanical performance, high ductility, and specifically superhardness, having potential applications as molecular sieves, shape-selective catalysts, absorbents, cutting tools, and coatings, among others. Also, nanocrystals of the superdense carbon with a bcc structure (bcc-C_8) were synthesized by a pulsed-laser induced liquid–solid interface reaction [50, 51]. The formed micro- and nanocubes are single crystals (Fig. 6.21) with a bcc structure with a lattice constant of 5.46 Å, having a slightly truncated shape bounded mainly by {200} facets. This carbon nanomaterial was found to be a semiconductor with blue luminescence.

The known carbon allotrope, 2D bcc-C_6 (Fig. 6.22, a metastable, body-centered carbon allotrope with six atoms per primitive unit), according to DFT calculations, should have exceptionally low-surface energy and little size dependence down to only a couple layer thickness [52], explained by the existence of the relatively-high-energy bcc-C_6 during growth. bcc-C_6 belongs to low-surface-energy allotropes but with much stronger layer–layer interaction than that in graphite. bcc-C_6 is more similar to the experimental superdense carbon than the previously proposed supercubane C_8.
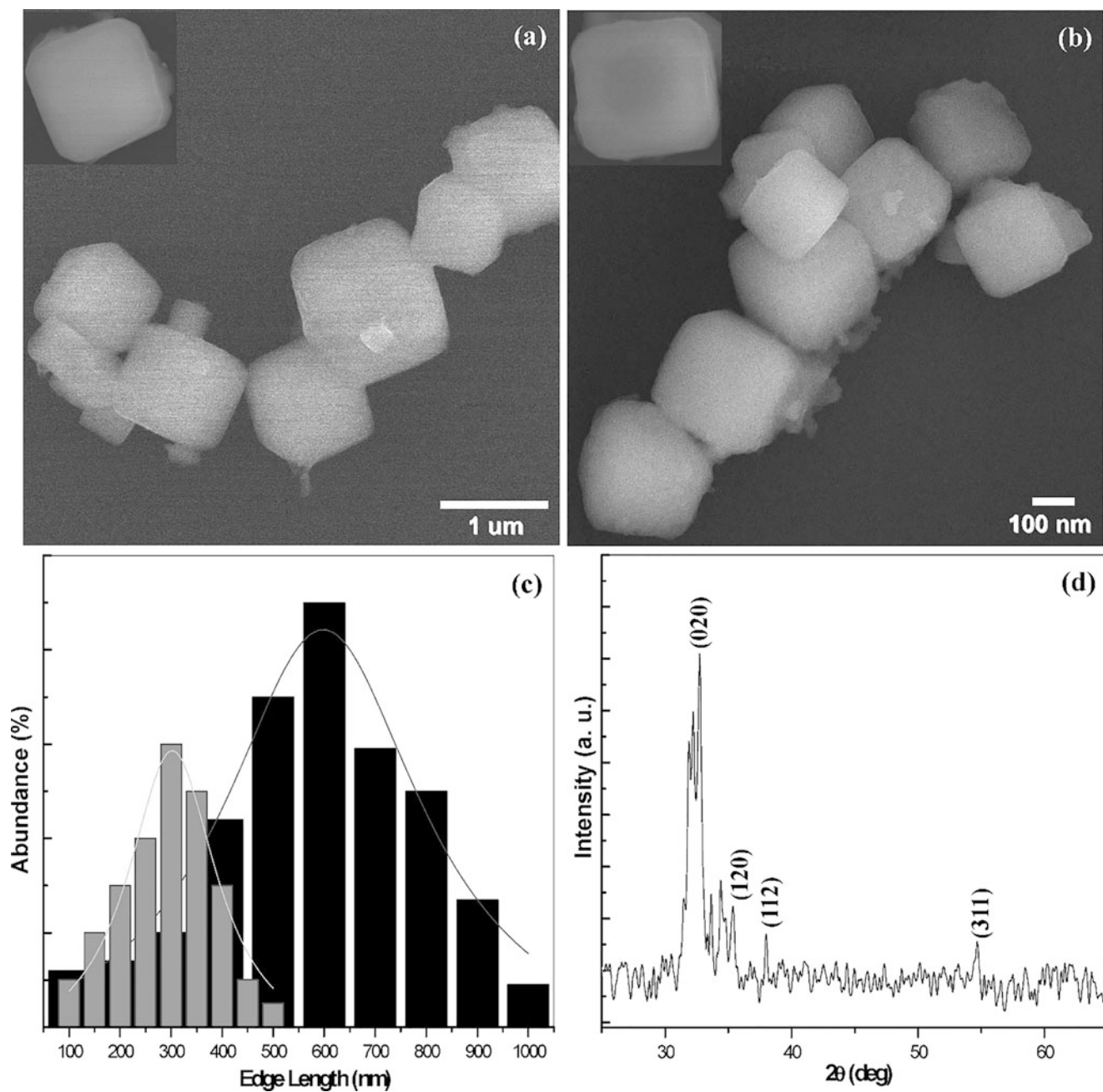
Fig. 6.21 SEM images of the synthesized carbon micro- and nanocubes (**a**, **b**) and the insets are high-magnification SEM images of slightly truncated carbon nanocube. Two distribution histograms of the size ration of cubes are shown in (**c**). The corresponding XRD pattern is shown in (**d**). (Reproduced with permission of the *American Chemical Society*)

Fig. 6.22 2D layered bcc-C$_6$ with (**a**) (111), (**b**) (110), and (**c**) (100) surfaces. Atoms in the first, middle, and third layers are shown in green, orange, and purple, respectively. (Reproduced with permission of the *Royal Society of Chemistry*)
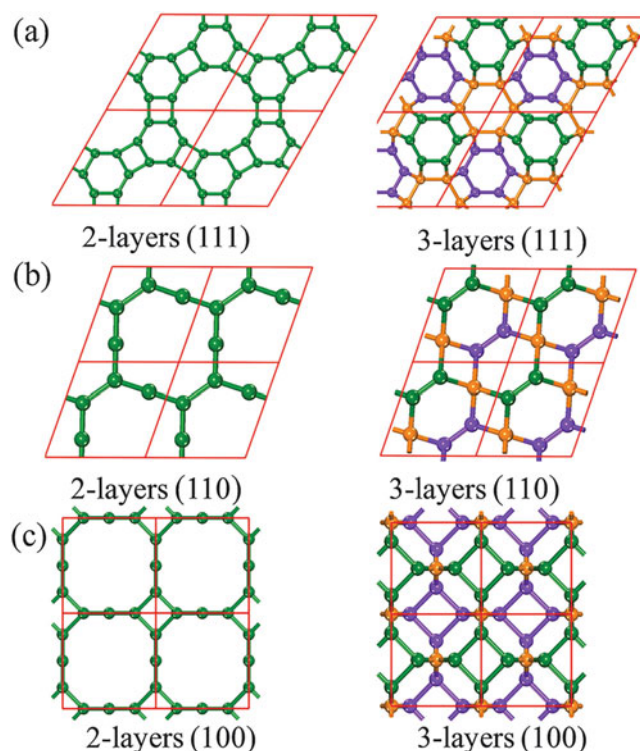
6.4   bct-Carbon[4]
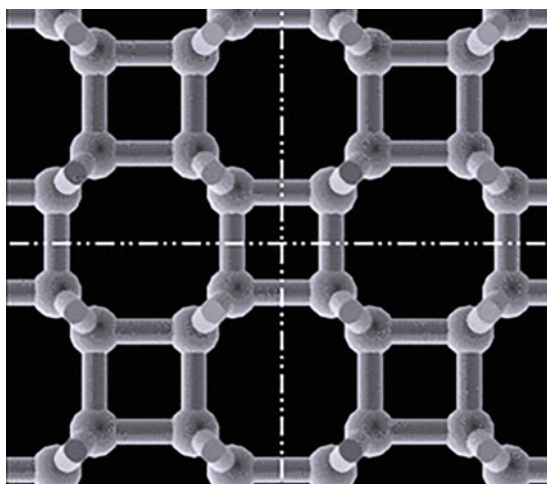
Body-centered tetragonal carbon (bct-carbon) was first proposed in 2010. The bct-C$_4$ phase (Fig. 6.23) is transparent and dynamically stable at zero pressure [53]. All carbon atoms are symmetrically equivalent, forming a structure closely related to those of graphite and hexagonal diamond. bct-C$_4$ is an accessible form of sp^3 carbon along the graphite-to-hexagonal diamond transformation path (Fig. 6.24) [54]. By rearranging half of carbon atoms, i.e., by changing the buckling pattern of these layers, bct-C$_4$ can be transformed into hexagonal diamond. In addition, bct-C$_8$ (Fig. 6.25) can be formed by sp^3-bonded carbon atoms and can be regarded as a compressed bundle of carbon nanotubes (CNTs) [55]. bct C$_8$ is a semiconductor with an indirect gap of 1.66 eV, can be transformed to semimetal being doping with boron and nitride atoms, and would have fruitful applications in carbon-based electronics and energy storage (Li storage), in case of its synthesis.

---

[4]Reproduced with permission of the *American Physical Society* (*Phys. Rev. B*, 2010, *82*, 134126).
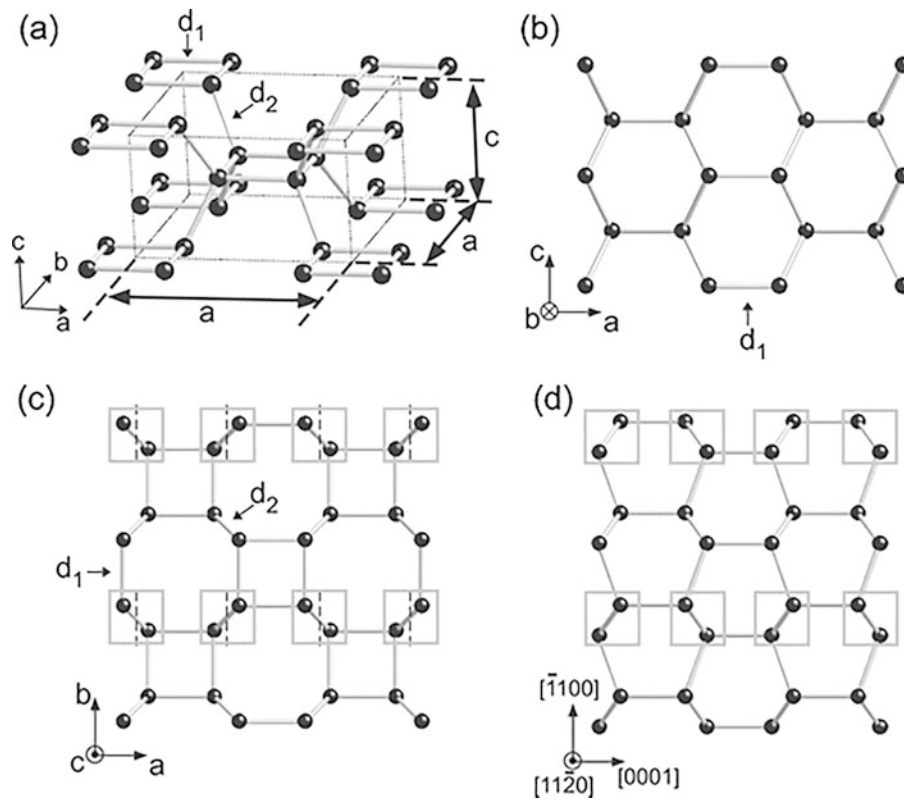
Fig. 6.23 Crystal structure of bct-C$_4$: (**a**) three-dimensional view, (**b**) view along the b axis, and (**c**) along the c axis. In (**c**), if pairs of carbon atoms in the gray boxes are flipped across the planes denoted by dashed lines, bct-C$_4$ transforms to (**d**) hexagonal diamond. (Reproduced with permission of the *American Physical Society*)
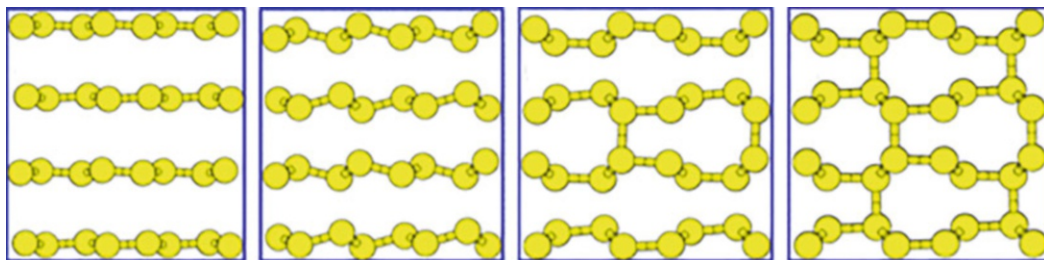

Fig. 6.24 Transition paths of bct-carbon under pressure of 20 GPa (Reproduced with permission of the *American Physical Society*)

Selected features of bct-carbon are as follows:

– bct-Carbon is crystalline with sp^3 configuration with body-centered tetragonal I4/mmm symmetry.
– bct-Carbon consists of sheets of squares of four carbon atoms each, joined by "short" bonds perpendicular to the sheets.
– It can be synthesized when graphite is exposed to high pressure at normal temperatures.
– Its shear strength is 17 percent greater than diamond's.
– It is more stable than graphite at 18.6 GPa.
– bct-Carbon has a higher shear strength than diamond due to its perpendicular graphene-like structure.
– bct-C$_4$ presents a super uniaxial compressive strength of 524.3 GPa, which is 6.9% more than the corresponding value of diamond [56]. The high compressive strength originates from the high compressive rate of chemical bond deviating from compressive direction.
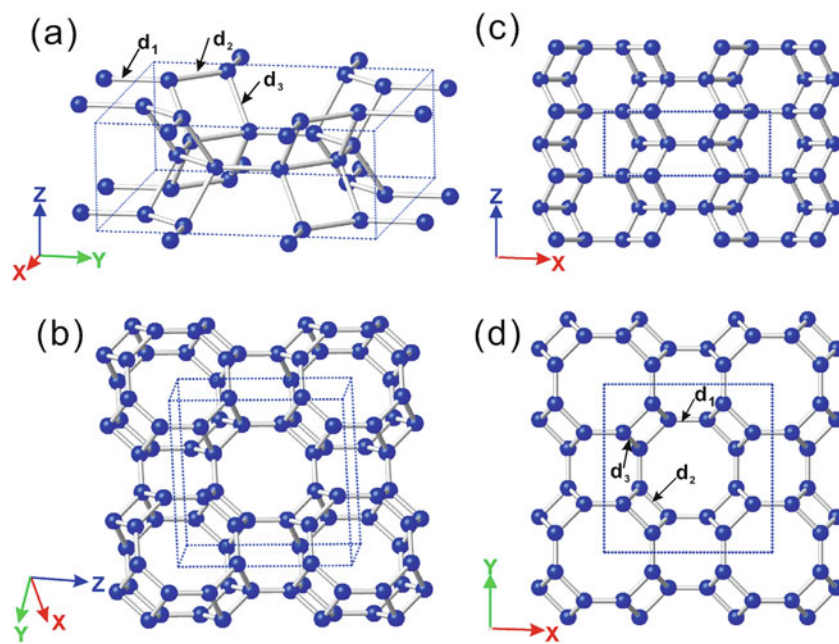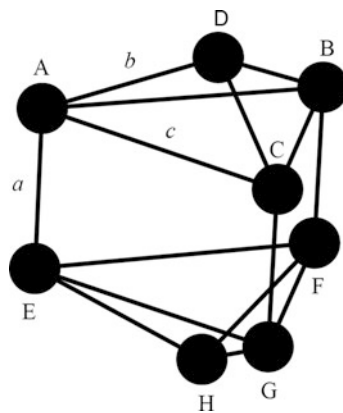
Fig. 6.25 Schematic drawing of the crystal structure of Bct C_8; (**a**) and (**b**) are the perfective views; (**c**) and (**d**) are the side view and the top view, respectively. The dash line indicates the unit cell. (Reproduced with permission of *Elsevier Science*)

6.5   Prismane C_8[5]

Prismane C_8 (Fig. 6.26; should not be confused with corresponding hydrocarbon with the same name) is a theoretically predicted metastable carbon allotrope. It consists of an atomic cluster of eight carbon atoms, with the shape of an elongated triangular bipyramid – a six-atom triangular prism with two more atoms above and below its bases [57, 58]. It possesses a rather high stability, the activation energy for prismane decay being about 0.8 eV. The prismane lifetime increases rapidly as the temperature decreases, indicating the possibility of experimental observation of this cluster.

---

[5]Reproduced with permission of *Springer* (*Journal of Experimental and Theoretical Physics Letters*, 1998, *68*(9), 726–731).

Fig. 6.26 A $(C_8)_5$ ensemble
consisting of 5 C_8 prismanes
[59]. (Reproduced with
permission of *Springer*)
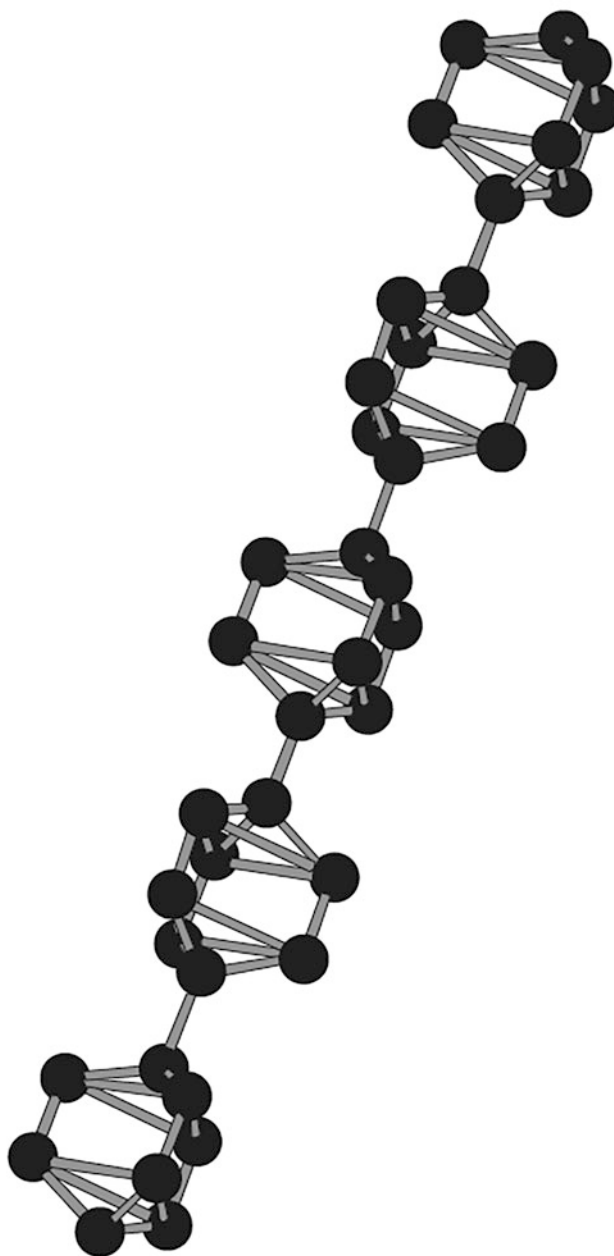
6.6   K4 Crystal
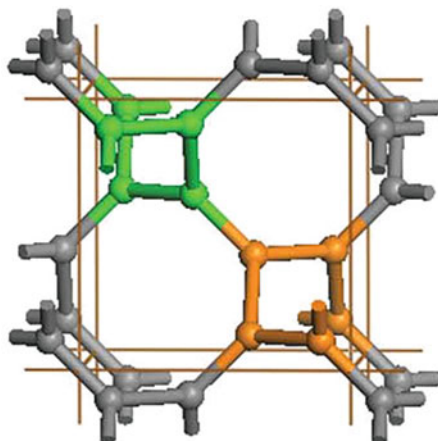
The *K*4 crystal is a theoretically predicted 3D crystalline metastable carbon structure, where each sp^2-hybridized carbon atom is bonded to three others, at 120° angles (like graphite) but where the bond planes of adjacent layers lie at an angle of 70.5°, rather than coinciding. Various physical properties of the K_4 carbon crystal, especially for the electronic properties, were evaluated by first-principles calculations [60]. A possible pressure-induced structural phase transition from graphite to K_4 was suggested. Twisted π states across the Fermi level resulted in metallic properties in this carbon crystal. Structural differences of diamond, graphite, and K_4 crystal are shown in Fig. 6.27. A significant difference is that the K4 crystal, with its three-coordinated and three-dimensional (3C-3D) structure, has chirality, while the diamond crystal [with tetracoordinated (4C)-3D structure] does not [61].

Fig. 6.27 Binding energy vs. volume curves of diamond (blue), graphite (grey and black), and K4 (red) crystal structures composed of carbon atoms based on (**a**) LDA and (**b**) GGA. (Reproduced with permission of the *American Physical Society*)
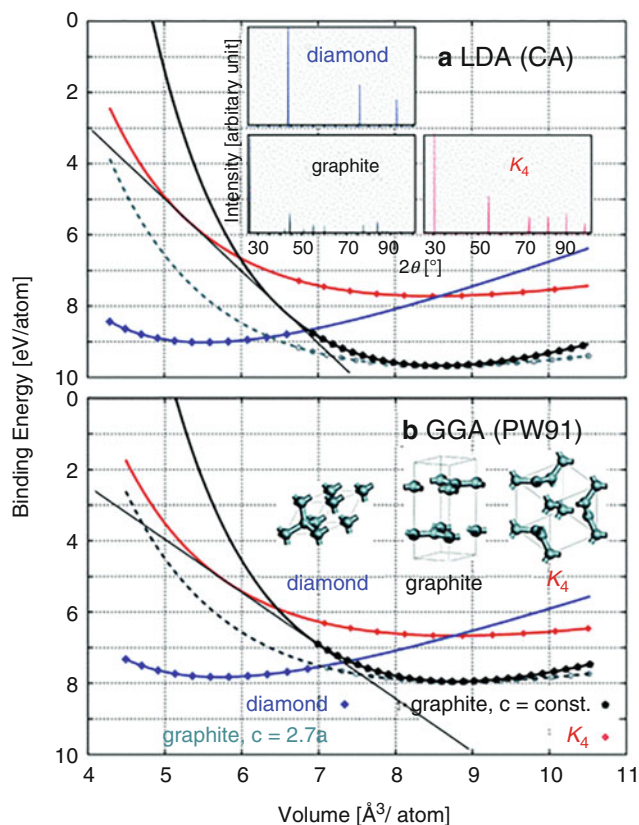
6.7 Penta-Graphene[6]
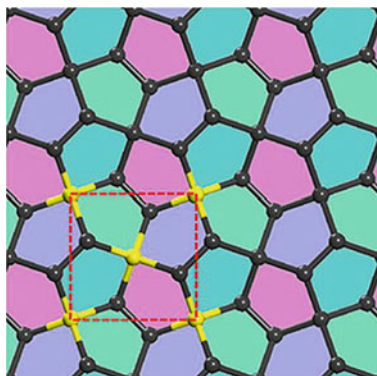
Whereas hexagons are the primary building blocks of many of carbon allotropes (except for C_{20} fullerene), carbon structures made exclusively of pentagons are not known. The penta-graphene, composed of only carbon pentagons and resembling Cairo pentagonal tiling, can be dynamically, thermally, and mechanically stable. Proposed in 2014, it is a carbon allotrope containing both sp^2- and sp^3-hybridized carbon atoms, composed entirely of carbon pentagons and resembling the Cairo pentagonal tiling. It is unstable in pure form but can be stabilized by hydrogenation resulting penta-graphane [62]. Several features of penta-graphene are as follows:

– It is dynamically stable and can withstand temperatures up to 1000 K, although it is energetically metastable compared with graphene.
– It exhibits negative Poisson's ratio, a large band gap, and an ultrahigh mechanical strength.
– Penta-graphene is an insulator with an indirect band gap of 4.1–4.3 eV.
– Its room-temperature thermal conductivity is about 167 W/mK [63], which is much lower than that of graphene.
– Penta-graphene can be rolled up to form a 1D pentagon-based nanotube and stacked to form 3D stable structures.
– It can be functionalized with hydrogen and other different functional groups, changing the failure stress, strain, and other properties [64–66].
– Penta-graphene is a promising anode material as the Li/Na-ion battery [67].

The data on penta-graphene stability are contradictory [68]. For example, as it was suggested, a 2D carbon sheet, penta-graphene (Fig. 6.28), composed entirely of pentagons, could be obtained by chemically exfoliating a single layer from the T12-carbon phase [69]. However, it was suggested and calculated by Kroto et al. [70] that penta-graphene will not be an

$d_1 = 1.535$ Å
$d_2 = 1.555$ Å
$h = 0.850$ Å

0.6 Å

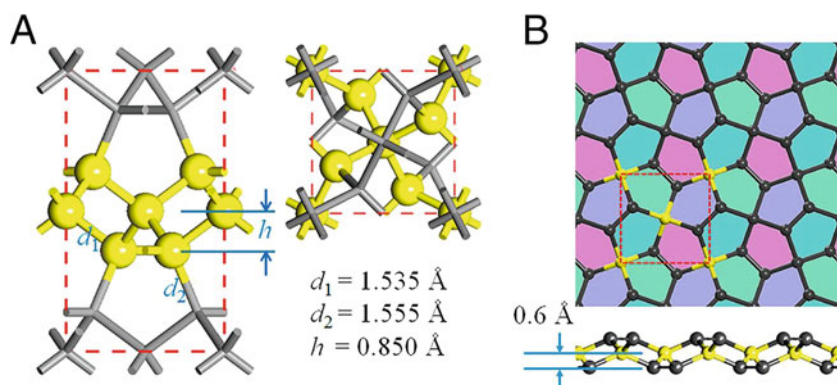**Fig. 6.28** (**a**) Crystal structure of T12-carbon viewed from the [100] and [001] directions, respectively. (**b**) Top and side views of the atomic configuration of penta-graphene. The square marked by red dashed lines denotes a unit cell, and the highlighted balls represent the sp^3 hybridized C atoms. (Reproduced with permission of *PNAS*)

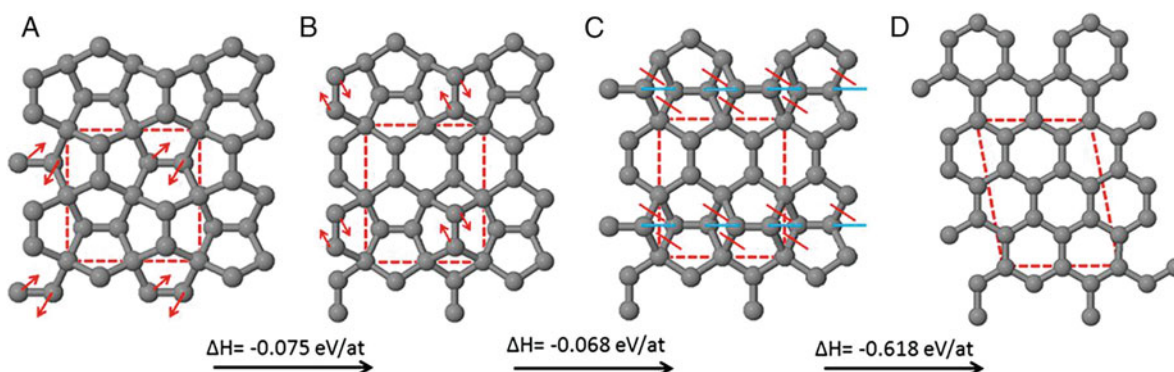[6]Reproduced with permission of *PNAS* (*PNAS*, 2015, *112*(8), 2372–2377).

Fig. 6.29 A calculated structural transformation route from (**a**) penta-graphene to (**d**) graphene; each step is exothermic. Red arrows indicate direction of motion of atoms for 90° rotation of carbon–carbon bonds. Red (blue) lines indicate C–C bonds that are broken (formed). Note that structures A–C were constrained within orthogonal unit cells; this constraint was lifted for step C to D. The final structure, graphene, is 0.761 eV per atom more stable than A. Unit cells are marked with dotted lines; calculated cell dimensions are (**a**) 5.095 × 5.095 Å, (**b**) 4.769 × 5.510 Å, (**c**) 4.888 × 5.318 Å, and (**d**) 4.883 × 6.476 Å, α = 100.88°. (Reproduced with permission of *PNAS*)

experimentally achievable allotrope of carbon. The problem is not only in its isolation among similar-energy isomers but also due to its rapid restructurization yielding graphene (Fig. 6.29) in presence of impurities as catalysts. At the same time, it was suggested that chiral penta-CNTs on penta-graphene basis are good candidates to be obtained experimentally. Thus, a computational study on the structure and electronic properties of penta-graphene nanotubes (penta-CNTs, Fig. 6.30), based on a periodic plane wave-pseudopotential approach, was carried out [71], considering chiral structures, among zigzag and armchair structures. In particular, it was revealed that the energetic stability (binding energy per atom or BEA) of chiral penta-CNTs is comparable with (n,n) penta-CNTs. In addition, penta-CNTs with reversed indexes (i.e., penta-CNTs with index (n, m) and (m,n)) are equal, because of their chiral angles which are comprised between 0 and 45 degrees. Mechanical properties of penta-graphene nanotubes [72] and its monolayer [73] were also studied. Finally, the mechanism of translation symmetry breakdown in penta-graphene with multiple sp^2/sp^3 sublattices was studied by GGA DFT, DFTB, and model potential approaches (Fig. 6.31) [74]. It was shown that 2D sp^2/sp^3 nanostructures are correlated transition states between two symmetrically equivalent bent structures. Strong mechanical stress prevents stabilization of the nanoclusters on any type of supports by either van der Waals or covalent bonding and should lead to formation of pentatubes, nanorings, or nanofoams rather than infinite nanoribbons or nanosheets. There are also other recent studies on approaches to penta-graphene models and its possible transformations [75, 76].

Fig. 6.30 Various penta-CNT structures. Red lines delimitate each unit cell, while the magnitude of its translational vector are shown under each nanotube. (Reproduced with permission of the *Elsevier Science*)
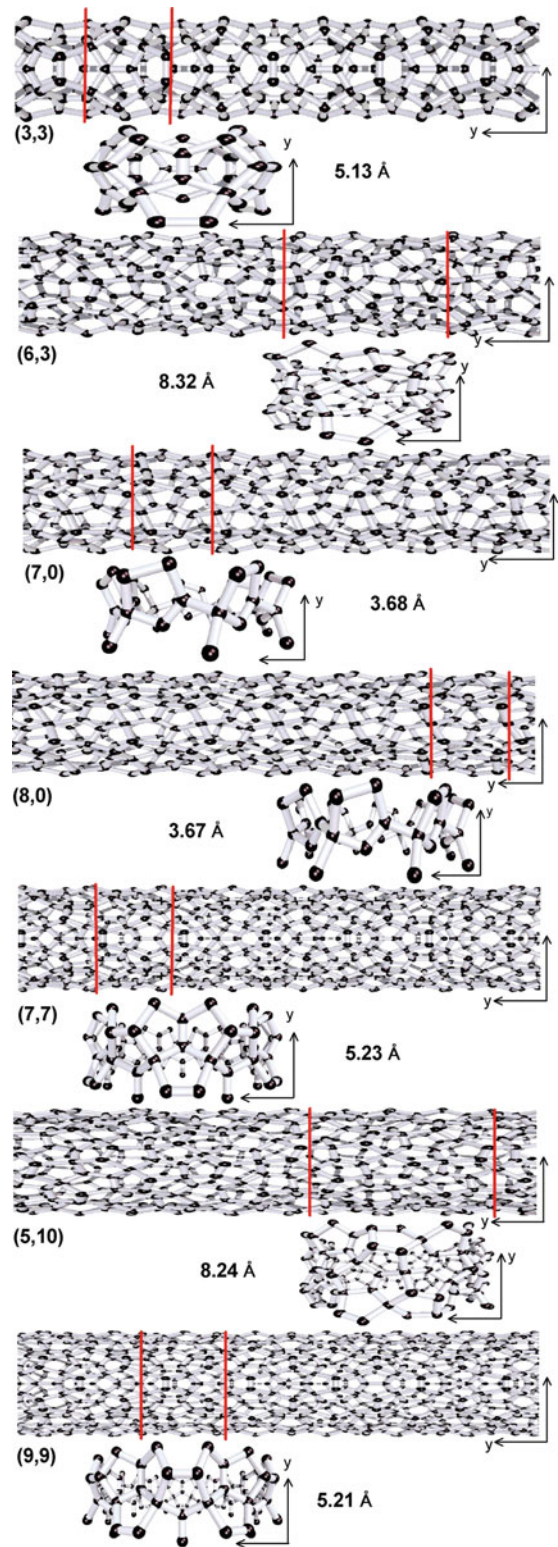
Fig. 6.31 Top (**a**) and side (**b**) projections of 2D penta-graphene and 1D pentaribbon (**c, d**) calculated using PBC approach. Carbon atoms of sp^3 sublattice are depicted in red, the sp^2 carbon dimers of the top and bottom subblattices are depicted in blue, and the unit cells of penta-graphene and pentaribbon are marked by green rectangles. (Reproduced with permission of the *American Chemical Society*)
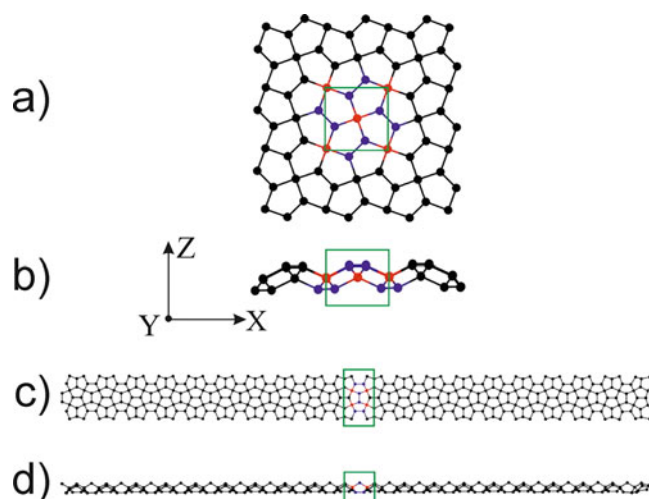
6.8 Haeckelites
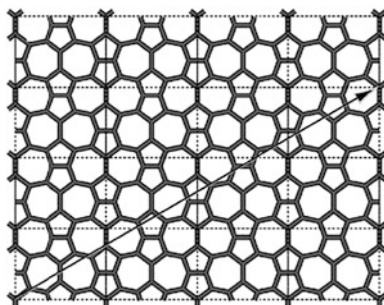
Haeckelites, first proposed by Terrones in 2000, are layered sp^2-like threefold coordinated networks of carbon atoms in 2D Bravais lattices, generated by a periodic arrangement of pentagons, hexagons, and heptagons. They can consist, in particular, of equal numbers of pentagons and heptagons, in addition to any number of hexagons. Similar atomic arrangements have been observed in 5–7 and 5–8 defect lines, among others. Some features of haeckelites are as follows:

– Haeckelites can be rolled so as to generate nanotubes of different diameter and chirality.
– Haeckelite structures were shown to be good candidates of conducting wires with great potential in nanoelectronics [77].
– Haeckelite sheets and tubes (Fig. 6.32) are metastable and more favorable than C_{60}; their mechanical properties are similar to those of graphene [78]. All structures, according to calculations, possess an intrinsic metallic behavior, independent of orientation, tube diameter, and chirality.

Starting from a planar Haeckelite array, tubular structures (Fig. 6.33) were obtained by applying the same wrapping procedure as for the usual nanotubes, which are rolled up sheets of graphene [79]. The haeckelite nanotubes may adopt various shapes, in particular coiled structures, double-screw molecules, corrugated cylinders, and pearl-necklace-like nanotubes. Studying lithium insertion to such haeckelite nanotubes, as well as to classic carbon nanotubes, it was revealed [80] that the metal interacts preferably with the pentagonal and heptagonal rings of the haeckelite rather than the hexagonal of the carbon nanotube. Haeckelites were found to be more promising materials for lithium storage applications (storing Li with a density of $LiC_{1.6}$) than carbon nanotubes. Among several other recent investigations on haeckelites, DFT structural studies together with DFT-based non-equilibrium Green function calculations were applied to investigate how the presence of non-hexagonal rings affects electronic transport in graphitic structures [81], resulting that infinite monolayers, finite-width nanoribbons, and nanotubes formed of 5–8 haeckelite with only five- and eight-membered rings are generally more conductive than their graphene-based counterparts.

Fig. 6.32 Haeckelite sheets consisting of various units cells: (**a**) rectangular _R5,7, (**b**) hexagonal _H5,6,7_, and (**c**) oblique _O5,6,7_. Nonchiral haeckelite tubes of similar diameters (ca. 1.4 nm) have been created using the three types of layered crystals: (**d**) R5,7 _6, 0_, (**e**) H5,6,7 _6, 0_, and (**f**) O5,6,7 _0, 8_ [Note: Subindices _5, 6, 7_ of the above structures indicate the presence of pentagonal, hexagonal, and heptagonal rings, respectively]. (Reproduced with permission of the *APS Physics*)
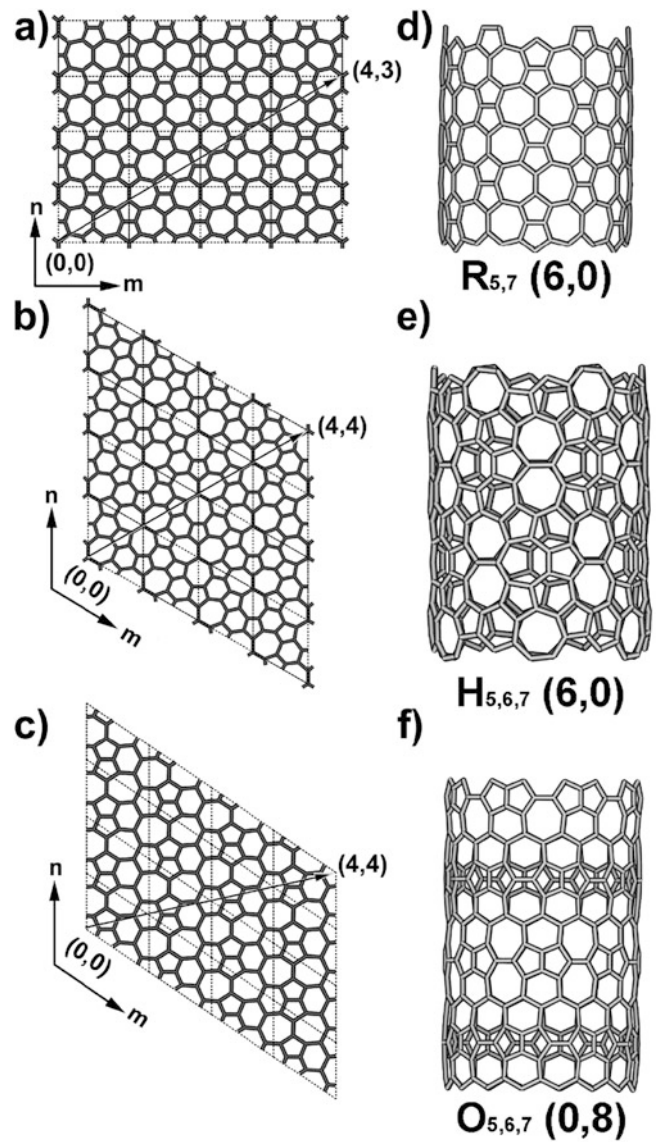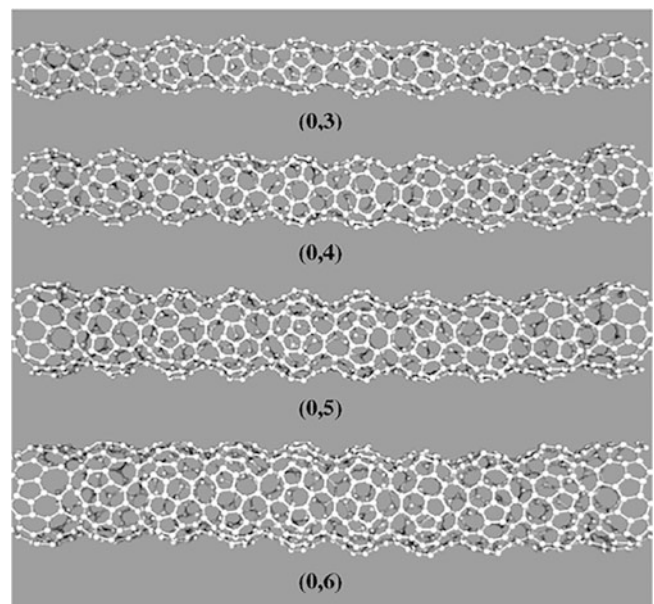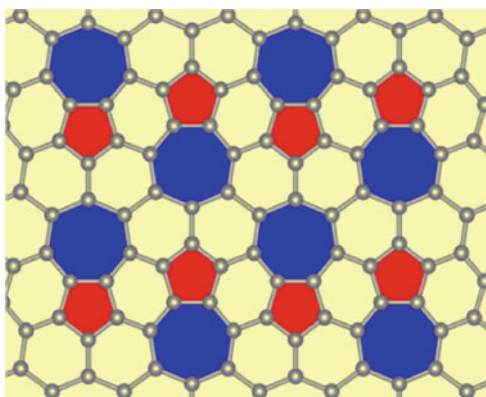

Fig. 6.33 Ball-and-stick representations of *(0,m)* nanotubes generated from the haeckelite stripe. (Reproduced with permission of the *IOP Publishing*)

6.9 Phagraphene

Among graphene allotropes, penta-graphene and phagraphene, the Haeckelite-like *Phagraphene*, proposed in 2015, is composed of 5-6-7 carbon rings (Fig. 6.34); it is only dynamically and thermally stable [82, 83]. Phagraphene, as well as graphene, is a material where Dirac cones appear, and electrons behave similar to particles without mass. In phagraphene, due to the different number of atoms in the rings, the Dirac cones are inclined. This 2D carbon structure with *Pmg* plane group is lower in energy than most of the predicted 2D carbon allotropes due to its sp^2-binding features and density of atomic packing comparable to graphene. Some features of phagraphene are as follows:
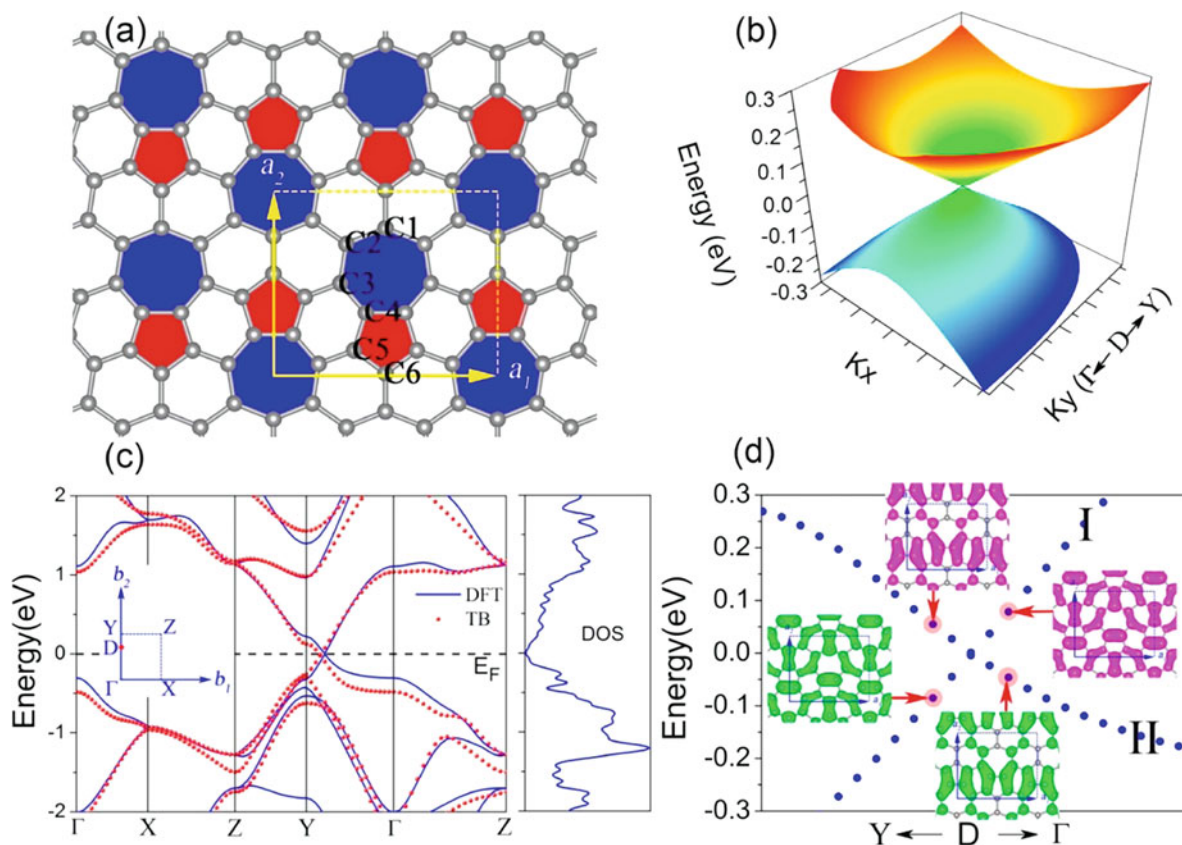
Fig. 6.34 (**a**) Structure of phagraphene with notable space-inversion symmetry, C1–C6 are unequivalent carbon atoms in its unit cell. (**b**) Distorted Dirac cone formed by the valence and conduction bands in the vicinity of the Dirac point. (**c**) Comparison of band structures from DFT (blue line) and TB (red circle) model. The corresponding DOS is zero at the Fermi level. Inserted first BZ with high symmetric k points: Γ (0,0,0), X (0.5,0,0), Z (0.5,0.5,0), Y (0,0,5,0), and Dirac point: D (0, 0.377,0). (**d**) Charge-density distributions near the distorted Dirac cone, both Dirac bands (denoted as I and II) are from *pz* orbitals of sp^2-carbon atoms. Fermi level has been set to zero. (Reproduced with permission of the *American Chemical Society*)

Fig. 6.35 Schematics of the atomic structures for penta-graphene and phagraphene. Unit cells are shown in pink. Side views of penta-graphene are shown on the top of this figure with three planes of atom (P1, P2, and P3). The atoms in P2 plane are marked in green. (Reproduced with permission of the *Royal Society of Chemistry*)

Fig. 6.36 A periodic supercell in the atomic structure of phagraphene. A 20-atom unit cell is also shown. In this study the properties are investigated along the armchair and zigzag directions. (Reproduced with permission of the *Royal Society of Chemistry*)
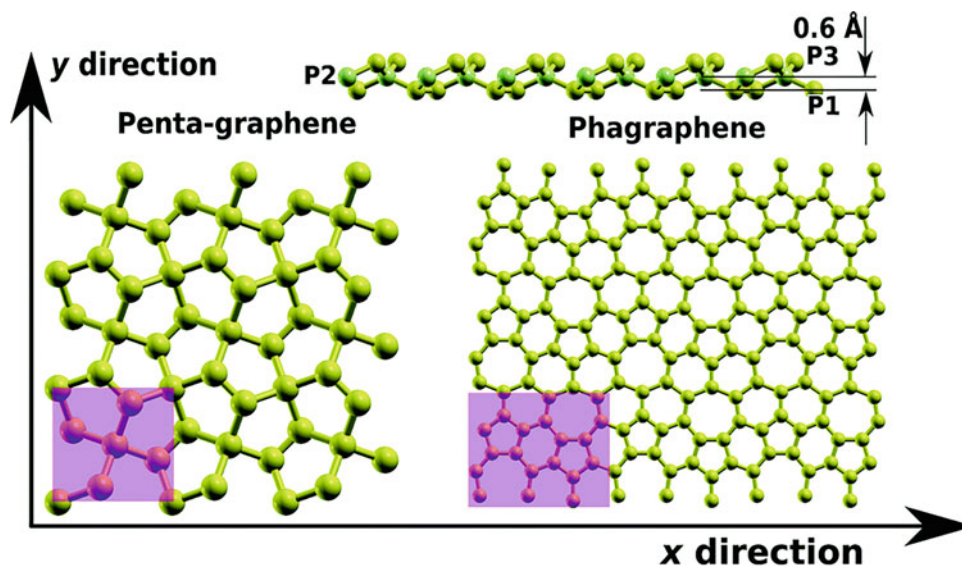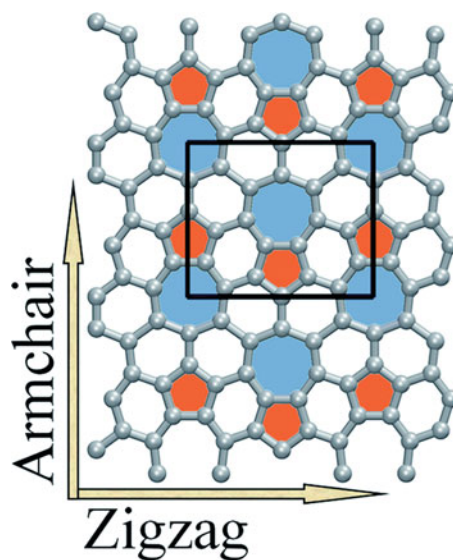

– Phagraphene is unstable or, at least, almost unstable with respect to transverse atomic displacements in the monolayer [84].
– Phagraphene has a potential energy of 193.2 kcal/mol.
– The bond order is 1.33, the same as for graphene.
– Phagraphene is considered an advanced material for flexible electronic devices, transistors, solar batteries, display units, and many other things.

DFT calculations were applied to evaluate the mechanical properties of penta-graphene and phagraphene (Fig. 6.35) and compared with graphene, graphane, and pentaheptite [73], resulting that the ultimate tensile strength (UTS) and the strain corresponding to UTS in both penta-graphene and phagraphene are smaller than that of graphene. Also, the charge density in sp^3 bonds is lower than that in the sp^2 bonds. In phagraphene, all the broken bonds were found to belong to the largest carbon ring in the structure. The thermal conductivity was found [85] to be anisotropic, with room-temperature values of 218 ± 20 W m^{-1} K^{-1} along the armchair direction and 285 ± 29 W m^{-1} K^{-1} along the zigzag direction (Fig. 6.36). Both values are one order of magnitude smaller than for pristine graphene.

Effects of Doping and Impurities A mixed-edge phagraphene ribbon was selected to study B-, N-, and BN-doping effects, respectively, on the geometric stability, electronic structure, carrier mobility, and device property [86]. These structures were found to be energetically stable. N or BN doping at different positions can modify the bandgap of ribbons, making ribbons become a wide, medium, or narrowed bandgap semiconductor. In case of silicon impurities, the structural, electronic, and magnetic properties were investigated systematically of pristine and Si-doped phagraphene nanoribbons (PHAGNRs) with different edges, including zigzag edge (ZPHAGNR) and mixed edge (MPHAGNR) [87]. It was revealed that the geometric structure is drastically changed when silicon atom replaces the different carbon atom on 5-6-7 rings of PHAGNRs. Among other effects, Si atom always prefers to substitute carbon atom at the edge position or on heptagon carbon ring both in 6-MPHAGNR and 4-ZPHAGNR. Also, DFT calculations on the lithium-ion storage capacity of two membranes, biphenylene (BP) membrane and phagraphene (PhG), showed a larger capacity than graphene, Li_2C_6, and $Li_{1.5}C_6$ compared to LiC_6 [88]. Li was found to be very mobile on these materials and does not interact as strongly with the membranes. Li atoms transfer a significant amount of charge to each of the membranes and that the bonding character is ionic.

Further Reading Stone–Wales defects in phagraphene [89]; simulation of the elastic properties of phagraphene [90]; modulation of the electronic and mechanical properties of phagraphene [91].

6.10 R3-Carbon[7]
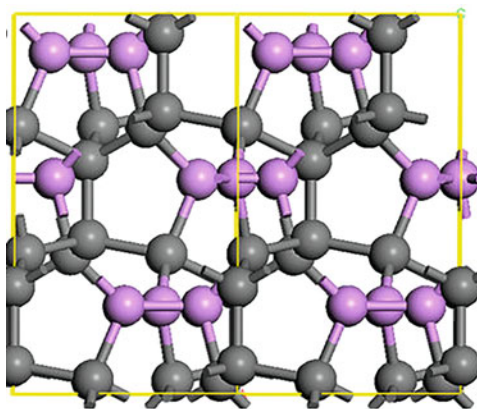
Phase transformation in glassy carbon (GC), simulated by means of DFT calculations in a wide range of pressures (0–79 GPa), revealed change in bonding type from *sp*- and sp^2-type to sp^3-type bonding [92], leading to a crystalline carbon allotrope possessing R3 symmetry (R3-carbon, Fig. 6.37). Its mechanical properties significantly vary due to the change of bonding type. With increasing pressure, the bulk moduli, shear moduli, and Young's moduli approach diamond values.

---

[7]Reproduced with permission of *Nature* (*Scientific Reports,* 2013, *3*, Article number: 1877).
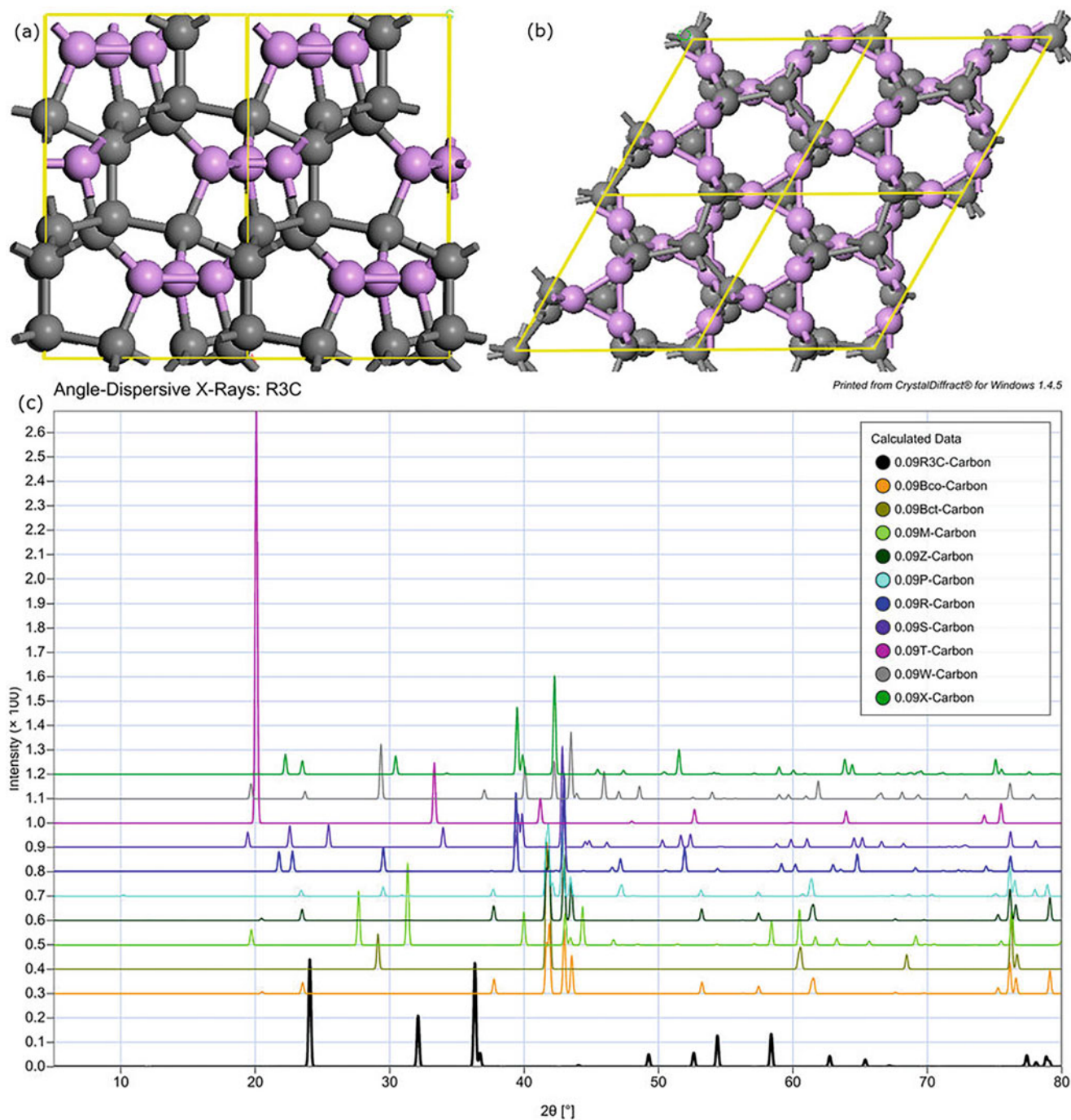
Fig. 6.37 (**a**) The R3-structure, the (001)-plane and the (010)-plane. Three-membered rings are colored in purple. (**b**) The calculated diffraction pattern of the R3 phase, Cco-C8 Carbon, Bct-Carbon, M-Carbon, Z-Carbon, P-Carbon, R-Carbon, S-Carbon, T-Carbon, W-Carbon, and X-Carbon, respectively. (Reproduced with permission of *Nature*)

6.11 *Imma*-Carbon
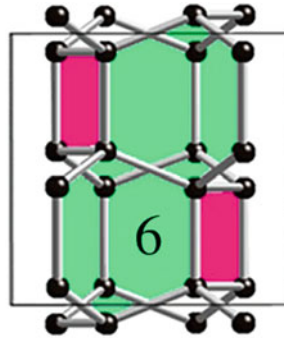
The polymorph sp^3 carbon allotrope, *Imma*-carbon (Fig. 6.38), is dynamically stable and a semiconductor with a direct band gap of ∼2.6 eV [93]. Calculations of bulk modulus and hardness indicate that this carbon is an ultra-incompressible and superhard material (bulk modulus of 444.7 GPa and a Vickers hardness of 83.5 GPa, which are larger than that of c-BN (66.3 GPa and 403.0 GPa)).
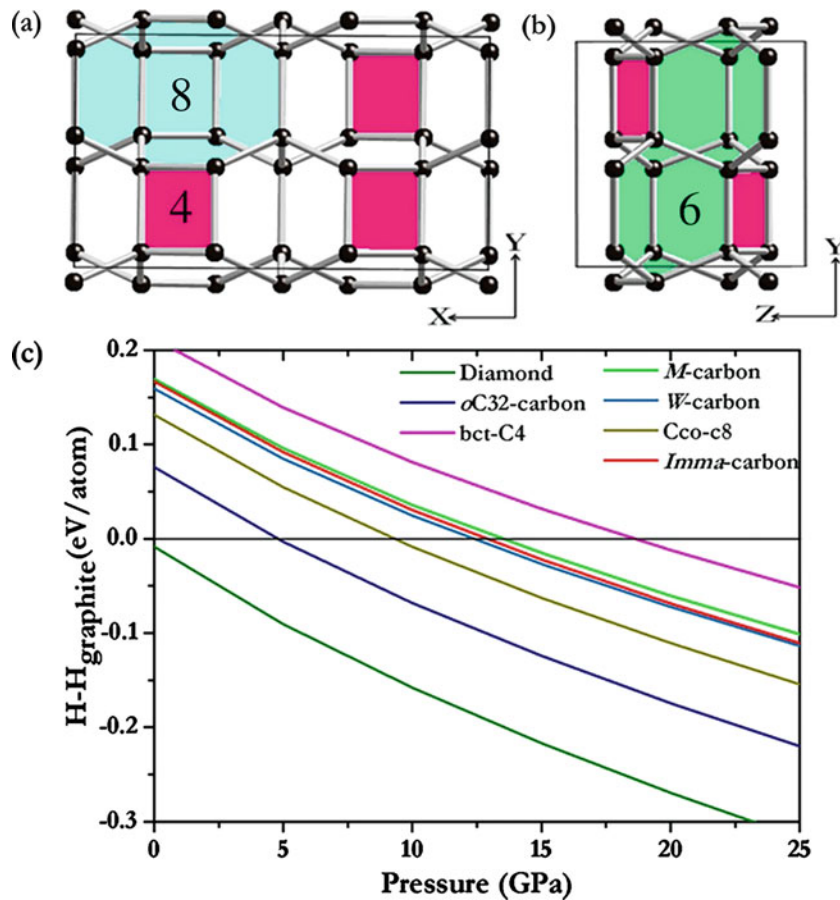
Fig. 6.38 (**a**, **b**) Polyhedral views of the crystal structure of *Imma*-carbon along two different directions, respectively. (**c**) Enthalpy differences of various carbon allotropes relative to graphite. (Reproduced with permission of the *Elsevier Science*)

6.12 I-Carbon[8]

I4-carbon was first proposed by Zhang et al. [15] This is a three-dimensional superhard carbon allotrope, which is confirmed to be thermodynamically, mechanically, and dynamically stable, having larger bulk modulus (393 GPa), shear modulus (421 GPa), *Young*'s modulus (931 GPa), and hardness (55.5 GPa), all of which are all slightly larger than those of c-BN. I4–carbon is an indirect bandgap semiconductor [94].
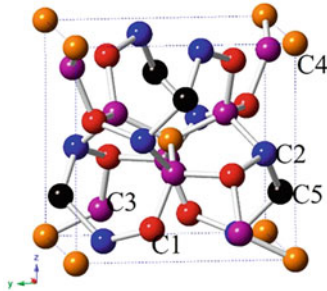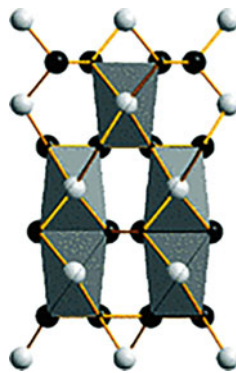
6.13 Superdense Carbon Allotropes

Searching for possible superdense carbon allotropes, three structures (*h*P3, *t*I12, and *t*P12, Fig. 6.39) were found [95] that have significantly greater density. The *h*P3 and *t*P12 phases have strong analogy with two polymorphs of silica (β-quartz and keatite), while the *t*I12 phase is related to the high-pressure SiS_2 polymorph. At ambient conditions, the *h*P3 phase is a semiconductor with the GW band gap of 3.0 eV, *t*I12 is an insulator with the bandgap of 5.5 eV, while *t*P12 is an insulator, the band gap of which is remarkably high (7.3 eV), making it the widest-gap carbon allotrope. These allotropes are metastable and have comparable to diamond or slightly higher-bulk moduli. Superdense carbon allotropes are predicted to have remarkably high refractive indices and strong dispersion of light. Authors believe that it is possible to obtain them by rapid dynamical compression of low-density forms of carbon. Alternatively, these allotropes can be synthesized by CVD techniques on a suitable substrate. Their dynamical stability indicates that, once synthesized, these allotropes can exist long at ambient conditions.

---

[8]Image reproduced with permission of the *MDPI* (*Materials*, 2016, *9*, 484, 15 pp.).
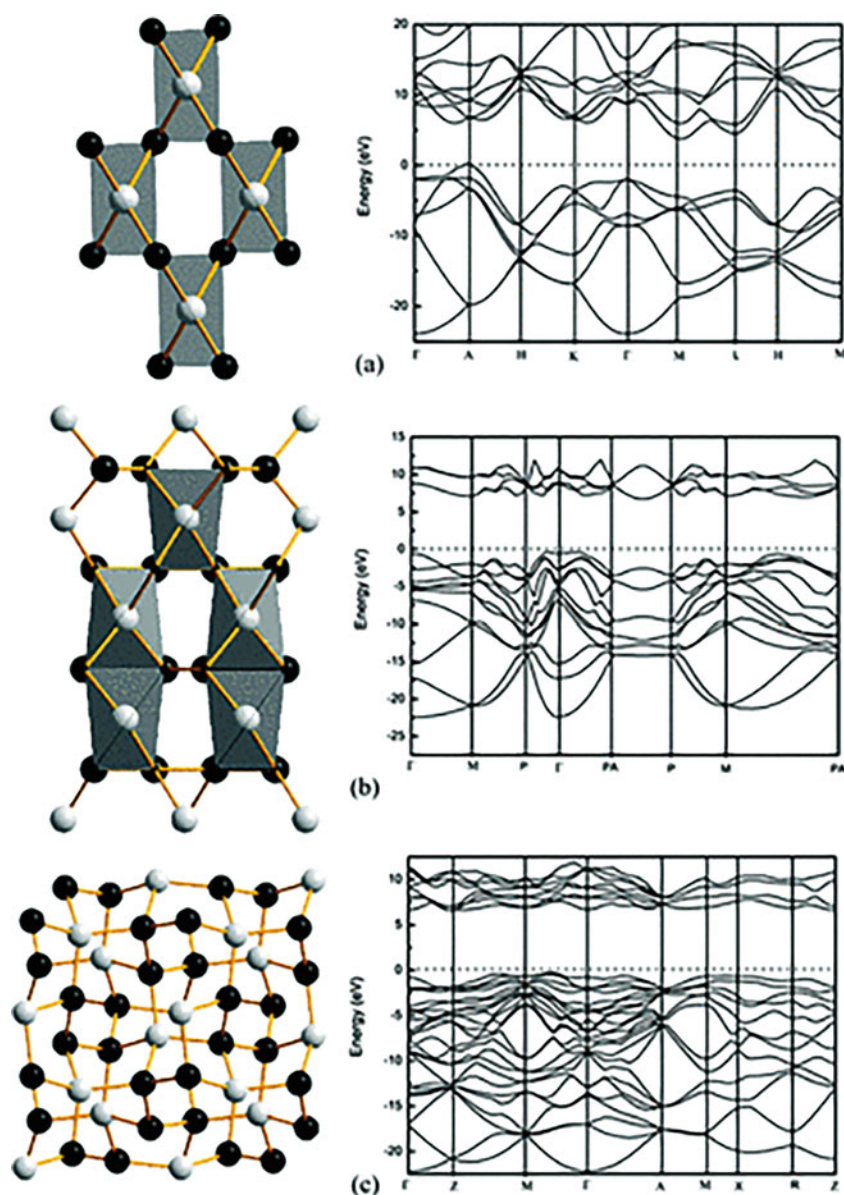
Fig. 6.39 Crystal structures and hybrid functional band structures of (**a**) *h*P3, (**b**) *t*I12, and (**c**) *t*P12 allotropes. For carbon allotropes, hybrid functional is believed to give the same level of accuracy as more rigorous GW quasiparticle calculations. The white (dark gray) spheres represent the different types of carbon atoms. (Reproduced with permission of *APS Physics*)

References

1. L.A. Burchfield, M. AlFahim, R.S. Wittman, F. Delodovicic, N. Manini, Novamene: a new class of carbon allotropes. Heliyon **3**(2), e00242 (2017)
2. F. Delodovicic, N. Manini, R.S. Wittman, Protomene: a new carbon allotrope. Carbon **126**, 574–579 (2018)
3. A.R. Oganov, C.W. Glass, Crystal structure prediction using ab initio evolutionary techniques: Principles and applications. J. Chem. Phys. **124**, 244704 (2006)
4. Q. Li, Y.M. Ma, A.R. Oganov, H.B. Wang, H. Wang, Y. Xu, T. Cui, H.K. Mao, G.T. Zou, Superhard monoclinic polymorph of carbon. Phys. Rev. Lett. **102**, 175506 (2009)
5. F. Tian, X. Dong, Z.S. Zhao, J.L. He, H.T. Wang, Superhard F-carbon predicted by ab initio particle-swarm optimization methodology. J. Phys. Condens. Matter **24**, 165504 (2012)
6. J.T. Wang, C. Chen, Y. Kawazoe, Low-temperature phase transformation from graphite to sp3 orthorhombic carbon. Phys. Rev. Lett. **106**, 075501 (2011)

7. Z.P. Li, F.M. Gao, Z.M. Xu, Strength, hardness, and lattice vibrations of Z-carbon and W-carbon: first-principles calculations. Phys. Rev. B **85**, 144115 (2012)

8. C.Y. He, L.Z. Sun, C.X. Zhang, X.Y. Peng, K.W. Zhang, J.X. Zhong, New superhard carbon phases between graphite and diamond. Solid State Commun. **152**, 1560–1563 (2012)

9. Q. Wei, M.G. Zhang, H.Y. Yan, Z.Z. Lin, X.M. Zhu, Structural, electronic and mechanical properties of *Imma*-carbon. EPL **107**, 27007 (2014)

10. C.Y. He, J.X. Zhong, M585, a low energy superhard monoclinic carbon phase. Solid State Commun. **181**, 24–27 (2014)

11. Z.S. Zhao, F. Tian, X. Dong, Q. Li, Q.Q. Wang, H. Wang, X. Zhong, B. Xu, D.L. Yu, J.L. He, et al., Tetragonal allotrope of group 14 elements. J. Am. Chem. Soc. **134**, 12362–12365 (2012)

12. M.J. Xing, B.H. Li, Z.T. Yu, Q. Chen, C2/m-carbon: structural, mechanical, and electronic properties. J. Mater. Sci. **50**, 7104–7114 (2015)

13. M.J. Xing, B.H. Li, Z.T. Yu, Q. Chen, Structural, elastic, and electronic properties of a new phase of carbon. Commun. Theor. Phys. **64**, 237–243 (2015)

14. Z.S. Zhao, B. Xu, X.F. Zhou, L.M. Wang, B. Wen, J.L. He, Z.Y. Liu, H.T. Wang, Y.J. Tian, Novel superhard carbon: C-centered orthorhombic C_8. Phys. Rev. Lett. **107**, 215502 (2011)

15. X.X. Zhang, Y.C. Wang, J. Lv, C.Y. Zhu, Q. Li, M. Zhang, Q. Li, Y.M. Ma, First-principles structural design of superhard materials. J. Chem. Phys. **138**, 114101 (2013)

16. J.-J. Zheng, X. Zhao, Y. Zhao, X. Gao, Two-dimensional carbon compounds derived from graphyne with chemical properties superior to those of graphene. Sci. Reports **3**, 1271 (2013)

17. Z. Li, M. Smeu, A. Rives, et al., Towards graphyne molecular electronics. Nat. Commun. **6**, 6321 (2014)

18. T. Belenkova, V. Chernov, V. Mavrinskii, Structures and electronic properties of graphyne layers. Mater. Sci. Forum **845**, 239–242 (2016)

19. R. Majidi, Electronic properties of porous graphene, α-graphyne, graphene-like, and graphyne-like BN sheets. Can. J. Phys. **94**(3), 305–309 (2016)

20. H. Lu, S.-D. Li, Two-dimensional carbon allotropes from graphene to graphyne. J. Mater. Chem. C **1**, 3677–3680 (2013)

21. Z. Li, Z. Liu, Z. Liu, Movement of Dirac points and band gaps in graphyne under rotating strain. Nano Res. **10**(6), 2005–2020 (2017)

22. W.-J. Yin, Y.-E. Xie, L.-M. Liu, et al., R-graphyne: a new two-dimensional carbon allotrope with versatile Dirac-like point in nanoribbons. J. Mater. Chem. A **1**, 5341–5346 (2013)

23. D. Solis, C.F. Woellner, D.D. Borges, D.S. Galvao, Mechanical and thermal stability of graphyne and graphdiyne nanoscrolls. arXiv:1701.05790, 2017. 0.1557/adv.2017.130

24. W. Wu, W. Guo, X. Cheng Zeng, Intrinsic electronic and transport properties of graphyne sheets and nanoribbons. Nanoscale **5**, 9264–9276 (2013)

25. L.D. Pan, L.Z. Zhang, B.Q. Song, S.X. Du, H.-J. Gao, Graphyne- and graphdiyne-based nanoribbons: density functional theory calculations of electronic structures. Appl. Phys. Lett. **98**, 173102 (2011)

26. S.W. Cranford, M.J. Buehler, Mechanical properties of graphyne. Carbon **49**, 4111–4121 (2011)

27. A. Ahmadi, M. Faghihnasiri, H. Ghorbani Shiraz, M. Sabeti, Mechanical properties of graphyne and its analogous decorated with Na and Pt. Superlattice. Microst. **101**, 602–608 (2017)

28. R. Couto, N. Silvestre, Finite element modelling and mechanical characterization of graphyne. J. Nanomater. **2016**., Article ID 7487049, 15 (2016)

29. J. Hou, Z. Yin, Y. Zhang, T. Chang, An analytical molecular mechanics model for elastic properties of graphyne-*n*. J. Appl. Mech. **82**(9.), 5 pp), 094501 (2015)

30. T. Ouyang, M. Hu, Thermal transport and thermoelectric properties of beta-graphyne nanostructures. Nanotechnology **25**(24), 245401 (2014)

31. N. Han, H. Liu, S. Zhou, J. Zhao, Possible formation of graphyne on transition metal surfaces: a competition with graphene from the chemical potential point of view. J. Phys. Chem. C **120**, 14699–14705 (2016)

32. Q. Yuan, F. Ding, Formation of carbyne and graphyne on transition metal surfaces. Nanoscale **6**, 12727–12731 (2014)

33. A. Saraiva-Souza, M. Smeu, L. Zhang, M.A. Ratner, H. Guo, Two-dimensional γ-Graphyne suspended on Si(111): a hybrid device. J. Phys. Chem. C **120**(8), 4605–4611 (2016)

34. B. Bhattacharya, U. Sarkar, Graphyne–graphene (nitride) heterostructure as nanocapacitor. Chem. Phys. **478**, 73–80 (2016)

35. S. Kim, J.Y. Lee, Doping and vacancy effects of graphyne on SO_2 adsorption. J. Colloid Interface Sci. **493**, 123–129 (2017)

36. R. Majidi, A.R. Karami, Adsorption of formaldehyde on graphene and graphyne. Phys. E **59**, 169–173 (2014)

37. D. Cortes-Arriagada, Adsorption of polycyclic aromatic hydrocarbons onto graphyne: comparisons with graphene. Int. J. Quantum Chem. **117**, e25346 (2017)

38. D. Zhang, J. Yang, E.H. Hasdeo, et al., Multiple electronic Raman scatterings in a single metallic carbon nanotube. Phys. Rev. B **93**, 245428 (2016)

39. T. Isoniemi, A. Johansson, J.J. Toppari, H. Kunttu, Collective optical resonances in networks of metallic carbon nanotubes. Carbon **63**, 581–585 (2013)

40. L. Liu, G.Y. Guo, C.S. Jayanthi, S.Y. Wu, Colossal paramagnetic moments in metallic carbon nanotori. Phys. Rev. Lett. **88**(21), 217206 (2002). 4 pp

41. H. Bu, M. Zhao, W. Dong, S. Lu, X. Wang, A metallic carbon allotrope with superhardness: a first-principles prediction. J. Mater. Chem. C **2**, 2751–2757 (2014)

42. Y. Cheng, R. Melnik, Y. Kawazoe, B. Wen, Three dimensional metallic carbon from distorting sp^3-bond. Cryst. Growth Des. **16**(3), 1360–1365 (2016)

43. S. Zhang, Q. Wang, X. Chen, P. Jena, Stable three-dimensional metallic carbon with interlocking hexagons. Proc. Natl. Acad. Sci. U. S. A. **110**(47), 18809–18813 (2013)

44. J. Liu, T. Zhao, S. Zhang, Q. Wang, A new metallic carbon allotrope with high stability and potential for lithium ion battery anode material. Nano Energy **38**, 263–270 (2017)

45. C.-X. Zhao, C.-Y. Niu, Z.-J. Qin, X.Y. Ren, et al., H_{18} carbon: a new metallic phase with sp^2-sp^3 hybridized bonding network. Sci. Rep. **6**, 21879 (2016)

46. A. Pokropivny, S. Volz, 'C$_8$ phase': supercubane, tetrahedral, BC-8 or carbon sodalite? Phys. Status Solidi B **249**(9), 1704–1708 (2012)
47. R.L. Johnston, R. Hoffmann, Superdense carbon, C$_8$: supercube or analog of .gamma.-silicon? J. Am. Chem. Soc. **111**(3), 810–819 (1989)
48. D. Sharapa, A. Hirsch, B. Meyer, T. Clark, Cubic C$_8$: an observable allotrope of carbon? Chem. Phys. Chem. **16**(10), 2165–2171 (2015)
49. M. Hu, F. Tian, Z. Zhao, et al., Exotic cubic carbon allotropes. J. Phys. Chem. C **116**(45), 24233–24238 (2012)
50. P. Liu, H. Cui, G.W. Yang, Synthesis of body-centered cubic carbon nanocrystals. Cryst. Growth Des. **8**(2), 581–586 (2008)
51. P. Liu, Y.L. Cao, C.X. Wang, X.Y. Chen, G.W. Yang, Micro- and nanocubes of carbon with C$_8$-like and blue luminescence. Nano Lett. **8**(8), 2570–2575 (2008)
52. W.J. Yin, Y.P. Chen, Y.E. Xie, L.M. Liu, S.B. Zhang, A low-surface energy carbon allotrope: the case for bcc-C$_6$. Phys. Chem. Chem. Phys. **17**(21), 14083–14087 (2015)
53. K. Umemoto, R.M. Wentzcovitch, S. Saito, T. Miyake, Body-centered tetragonal C$_4$: a viable sp^3 carbon allotrope. Phys. Rev. Lett. **104**, 125504 (2010)
54. X.-F. Zhou, G.-R. Qian, X. Dong, L. Zhang, Y. Tian, H.-T. Wang, *Ab initio* study of the formation of transparent carbon under pressure. Phys. Rev. B **82**, 134126 (2010)
55. H.-J. Cui, Q.-B. Yan, X.-L. Sheng, et al., The geometric and electronic transitions in body-centered-tetragonal C8: a first principle study. Carbon **120**, 89–94 (2017)
56. L. Qing-Kun, Y. Sun, Y. Zhou, F.L. Zeng, First principles study of the uniaxial compressive strength of bct-C4 carbon allotrope. Acta Phys. Sin. **61**(9), 093104 (2012)
57. L.A. Openov, V.F. Elesin, Prismane C$_8$: a new form of carbon? J. Exp. Theor. Phys. Lett. **68**(9), 726–731 (1998)
58. V.F. Elesin, A.I. Podlivaev, L.A. Openov, Meta-stability of the three-dimensional carbon cluster Prismane. Phys. Low-Dim. Struct. **11/12**, 91 (2000)
59. N.N. Degtyarenko, V.F. Elesin, N.E. L'vov, L.A. Openov, A.I. Podlivaev, Metastable quasi-one-dimensional ensembles of C$_8$ clusters. Phys. Solid State **45**(5), 1002–1003 (2003)
60. M. Itoh, M. Kotani, H. Naito, et al., New metallic carbon crystal. Phys. Rev. Lett. **102**, 055703 (2009)
61. N.U. Zhanpeisov, Theoretical DFT study on structure and chemical activity of new carbon K4 clusters. Res. Chem. Intermed. **39**, 2141–2148 (2013)
62. H. Einollahzadeh, S. Mahdi Fazeli, R. Sabet Dariani, Studying the electronic and phononic structure of penta-graphane. Sci. Technol. Adv. Mater. **17**(1), 610–617 (2016)
63. W. Xu, G. Zhang, B. Li, Thermal conductivity of penta-graphene from molecular dynamics study. J. Chem. Phys. **143**, 154703 (2015)
64. Y. Zhang, Q. Pei, Z. Sha, Y. Zhang, H. Gao, Remarkable enhancement in failure stress and strain of penta-graphene via chemical functionalization. Nano Res. **10**(11), 3865–3874 (2017)
65. S. Ebrahimi, Effect of hydrogen coverage on the buckling of penta-graphene by molecular dynamics simulation. Mol. Simul. **42**(17), 1485–1489 (2016)
66. X. Wu, V. Varshney, J. Lee, T. Zhang, et al., Hydrogenation of Penta-graphene leads to unexpected large improvement in thermal conductivity. Nano Lett. **16**(6), 3925–3935 (2016)
67. B. Xiao, Y.-c. Li, X.-f. Yu, J.-b. Cheng, Penta-graphene: a promising anode material as the Li/Na-ion battery with both extremely high theoretical capacity and fast charge/discharge rate. ACS Appl. Mater. Interfaces **8**(51), 35342–35352 (2016)
68. B. Rajbanshi, S. Sarkar, B. Mandal, P. Sarkar, Energetic and electronic structure of penta-graphene nanoribbons. Carbon **100**, 118–125 (2016)
69. S. Zhang, J. Zhouc, Q. Wang, et al., Penta-graphene: a new carbon allotrope. PNAS **112**(8), 2372–2377 (2015)
70. C.P. Ewels, X. Rocquefelte, H.W. Kroto, et al., Predicting experimentally stable allotropes: instability of penta-graphene. PNAS **112**(51), 15609–15612 (2015)
71. J.J. Quijano-Briones, H.N. Fernández-Escamilla, A. Tlahuice-Flores, Chiral penta-graphene nanotubes: structure, bonding and electronic properties. Comput. Theor. Chem. **1108**, 70–75 (2017)
72. M. Chen, H. Zhan, Y. Zhu, H. Wu, Y. Gu, Mechanical properties of Penta-graphene nanotubes. J. Phys. Chem. C **121**(17), 9642–9647 (2017)
73. H. Sun, S. Mukherjee, C. Veer Singh, Mechanical properties of monolayer penta-graphene and phagraphene: a first-principles study. Phys. Chem. Chem. Phys. **18**, 26736–26742 (2016)
74. P. Avramov, V. Demin, M. Luo, et al., Translation symmetry breakdown in low-dimensional lattices of pentagonal rings. J. Phys. Chem. Lett. **6**(22), 4525–4531 (2015)
75. T. Stauber, J.I. Beltrán, J. Schliemann, Tight-binding approach to pentagraphene. Sci. Rep. **6**(22672), 8 (2016)
76. O. Rahaman, B. Mortazavi, A. Dianat, G. Cuniberti, T. Rabczuk, Metamorphosis in carbon network: from penta-graphene to biphenylene under uniaxial tension. FlatChem **1**, 65–73 (2017)
77. X. Rocquefelte, G.-M. Rignanese, V. Meunier, et al., How to identify Haeckelite structures: a theoretical study of their electronic and vibrational properties. Nano Lett. **4**(5), 805–810 (2004)
78. H. Terrones, M. Terrones, E. Hernández, N. Grobert, J.C. Charlier, P.M. Ajayan, New metallic allotropes of planar and tubular carbon. Phys. Rev. Lett. **84**, 1716 (2000)
79. P. Lambin, L.P. Biró, Structural properties of Haeckelite nanotubes. New J. Phys. **5**, 141 (2003)
80. G. Mpourmpakis, G.E. Froudakis, Haeckelites: a promising anode material for lithium batteries application. An *ab initio* and molecular dynamics theoretical study. Appl. Phys. Lett. **89**, 233125 (2006)
81. Z. Zhu, Z.G. Fthenakis, D. Tomanek, Electronic structure and transport in graphene/haeckelite hybrids: an *Ab Initio* study. arXiv:1502.07050, 2015; 2D Mater. 2015, 2, 035001
82. Z. Wang, X.-F. Zhou, X. Zhang, et al., Phagraphene: a low-energy graphene allotrope composed of 5–6–7 carbon rings with distorted dirac cones. Nano Lett. **15**(9), 6182–6186 (2015)
83. Z. Wang, X.-F. Zhou, X. Zhang, et al., Phagraphene: a low-energy graphene allotrope composed of 5-6-7 carbon rings with distorted dirac cones. arXiv:1506.04824, 2015
84. A.I. Podlivaev, L.A. Openov, Possible nonplanar structure of phagraphene and its thermal stability. *Pis'ma v Zh. Èksper. Teoret. Fiz.* **103**(3), 204–208 (2016)

85. L.F.C. Pereira, B. Mortazavi, M. Makaremic, T. Rabczukde, Anisotropic thermal conductivity and mechanical properties of phagraphene: a molecular dynamics study. RSC Adv. **6**, 57773–57779 (2016)
86. A.Y. Luo, R. Hu, Z.Q. Fan, H.L. Zhang, J.H. Yuan, C.H. Yang, Z.H. Zhang, Electronic structure, carrier mobility and device properties for mixed-edge phagraphene nanoribbon by hetero-atom doping. Org. Electron. **51**, 277–286 (2017)
87. Y. Liu, Z. Chen, S. Hu, G. Yu, Y. Peng, The influence of silicon atom doping phagraphene nanoribbons on the electronic and magnetic properties. Mater. Sci. Eng. B **220**, 30–36 (2017)
88. D. Ferguson, D.J. Searles, M. Hankel, Biphenylene and phagraphene as lithium ion battery anode materials. ACS Appl. Mater. Interfaces **9**(24), 20577–20584 (2017)
89. L.A. Openov, A.I. Podlivaev, Various stone–wales defects in phagraphene. Phys. Solid State **58**(8), 1705–1710 (2016)
90. L.A. Openov, A.I. Podlivaev, Negative poisson's ratio in a nonplanar phagraphene. Phys. Solid State **59**(6), 1267–1269 (2017)
91. D. Wu, S. Wang, J. Yuan, B. Yang, H. Chen, Modulation of the electronic and mechanical properties of phagraphene via hydrogenation and fluorination. Phys. Chem. Chem. Phys. **19**, 11771–11777 (2017)
92. X. Jiang, C. Århammar, P. Liu, J. Zhao, R. Ahuja, The R3-carbon allotrope: a pathway towards glassy carbon under high pressure. Sci. Rep. **3**, 1877 (2013)
93. Y. Liu, M. Lu, M. Zhang, First-principles study of a novel superhard sp^3 carbon allotrope. Phys. Lett. A **378**(45), 3326–3330 (2014)
94. M. Xing, B. Li, Z. Yu, Q. Chen, A reinvestigation of a superhard tetragonal sp^3 carbon allotrope. Materials **9**, 484 (2016). 15 pp
95. Q. Zhu, A.R. Oganov, M.A. Salvadó, P. Pertierra, A.O. Lyakhov, Denser than diamond: Ab initio search for superdense carbon allotropes. Phys. Rev. B **83**, 193410 (2011)